Wu Guo-Xiong (Orcid ID: 0000-0002-1838-1951)

Liu Yimin (Orcid ID: 0000-0002-5050-1642)

Jiang Zhihong (Orcid ID: 0000-0001-7864-2300)

# PV–Q Perspective of Cyclogenesis and Vertical Velocity Development Downstream of the Tibetan Plateau

Guoxiong Wu[1,2], Tingting Ma[1,3], Yimin Liu[♀,1,2,4], and Zhihong Jiang[3]

[1]State Key Laboratory of Numerical Modeling for Atmospheric Sciences and Geophysical Fluid Dynamics (LASG), Institute of Atmospheric Physics (IAP), Chinese Academy of Sciences (CAS), Beijing 100029, China. [2]College of Earth Science, University of Chinese Academy of Sciences, Beijing 100049, China. [3]Key Laboratory of Meteorological Disaster of Ministry of Education (KLME)/ Collaborative Innovation Center on Forecast and Evaluation of Meteorological Disasters (CIC-FEMD), Nanjing University of Information Science and Technology, Nanjing 210044, China. [4]CAS Center for Excellence in Tibetan Plateau Earth Sciences, Beijing 100101, China.

***Submitted to: Journal of Geophysical Research - Atmosphere***

**Key points:**

♀**Corresponding author:** Dr. Yimin Liu (lym@lasg.iap.ac.cn)

This article has been accepted for publication and undergone full peer review but has not been through the copyediting, typesetting, pagination and proofreading process which may lead to differences between this version and the Version of Record. Please cite this article as doi: 10.1029/2019JD030912

- Development of the omega equation is reviewed
- Impact of large-scale mountains on downstream cyclogenesis is considered from the perspective of potential vorticity and diabatic heating
- Feedback of diabatic heating on vertical velocity and potential vorticity advection during the cyclone life cycle is investigated

**Plain Language Summary**

Based on a brief review of the development of vertical velocity equation, a modified equation for the vertical velocity that is associated with the development of thermal field is deduced to link with condensation heating and horizontal transport/advection of potential vorticity (PV, a quantity measuring the potential of vorticity development). It is applied to interpret the cyclogenesis and associated severe precipitation downstream of the Tibetan Plateau in a winter case-study. Results demonstrate that the cyclogenesis is strongly tied both to the PV generation near the surface of the eastern Tibetan Plateau and to its subsequent downstream eastward advection. The latter triggers the development and interaction of various vertical velocity components, air convergence and cyclogenesis in the lower-troposphere, leading to precipitation and condensation heating. The life cycle of cyclogenesis is controlled by the vertical coupling between the zonal positive PV advection in the mid-troposphere and the meridional negative PV advection in the lower-troposphere. The heating in return can influence PV advection and vertical velocity development.

It is the vertical variation of horizontal PV advection and interaction with condensation heating that control the development of vertical velocity, the evolution of cyclogenesis and the associated precipitation downstream of the Tibetan Plateau.

**Abstract**

This study reviews the development of the omega equation and the relation between omega and potential vorticity (PV) advection, and considers the application of PV theory to investigate the impact of large-scale mountains on downstream weather development. A diabatic quasi-geostrophic omega equation is introduced to reveal the feedback of diabatic heating (Q) on PV advection and vertical velocity. A challenge therein concerning the use of the diagnostic omega equation to interpret weather system development is considered from the PV–Q perspective based on a severe weather event that occurred downstream of the Tibetan Plateau (TP) on 17–21 January 2008. Results demonstrate that owing to PV restructuring, positive PV was generated over the eastern flank of the TP, and its eastward advection triggered development of isentropic displacement vertical velocity and cyclogenesis in the lower troposphere. A converging southeasterly wind accompanied with ascending isentropic gliding vertical velocity in the lower troposphere was induced to the east of the cyclone center, which transported not only warm moist air but also negative PV from the south, contributing to developments of both local diabatic ascent and precipitation and eastward migration of the cyclone. During the cyclone life cycle, three omega components induced by different processes interacted with each other, and diabatic heating associated with precipitation exerted considerable feedback to vertical motion as well as PV advection. It is the vertical differential PV advection and feedback from diabatic heating that control the evolution of the circulation and the associated precipitation downstream of the TP.

**Keywords:** PV restructuring and PV advection, omega equation, feedback of diabatic heating Q, Tibetan Plateau, cyclogenesis

## 1 Introduction

Among various significant achievements in atmospheric sciences in the previous century, the developments of the omega equation and potential vorticity (PV) theory represent the two fundamental accomplishments in relation to extratropical weather and climate dynamics. Applying these established theories to interpret the impacts of orography on weather and climate has significantly advanced our understanding of the effects of mountains, which has contributed to the improvement of both weather forecasts and climate prediction.

### 1.1 Omega equation

Accurate diagnosis of vertical velocity has long been one of the challenging issues for meteorologists. With the application of quasi-geostrophic theory in meteorology, various forms of the omega equation have been used to interpret the vertical motion of systems (e.g., Sutcliffe, 1947; Bushby, 1952). Progressive studies linked vertical velocity with the advection of vorticity in the upper troposphere and the Laplacian of thermal advection (Petterssen, 1956; Djuric, 1969; Holton, 1972). For a diabatic atmosphere, the conventional omega equation in p-coordinates can be expressed as (Holton, 2004):

$$\mathrm{L}\{\omega\} = [\Sigma^2\nabla_h^2 + f^2\frac{\partial^2}{\partial p^2}]\omega = f\frac{\partial}{\partial p}(\vec{V}_g\cdot\nabla\eta_g) + \Pi(p)\nabla_h^2(\vec{V}_g\cdot\nabla\theta) - \Pi(p)\nabla_h^2\dot{\theta}, \quad (1)$$

where the parameters are:

$$\begin{cases}\Sigma^2 = \Sigma^2(p) = -\Pi(p)\Theta_p \\ \Pi(p) = \dfrac{R}{p}(\dfrac{p}{p_0})^{\kappa}\end{cases}. \quad (2)$$

In the above, $\dot{\theta}$ is diabatic heating rate ($\dot{\theta} = \frac{d\theta}{dt} = Q$), $\vec{V}_g = \vec{k}\times f^{-1}\nabla\Phi$ is geostrophic wind, $\eta_g = f + f^{-1}\nabla^2\Phi$ is absolute geostrophic vorticity, $\Theta(p)$ is a standard potential temperature distribution averaged over a horizontal domain and a period of interest, $\Theta_p$ is its

vertical gradient, and the other parameters are used following their conventional meteorological notation. This equation provides a basis for understanding the dynamics of mid-latitude weather systems. Each term on the right-hand side of Eq. (1) has clear interpretation as a separate physical process, i.e., increase with height of absolute vorticity advection, or warm advection, or diabatic heating will lead to ascent of air. However, in practice there is a drawback when diagnosing the individual forcing terms in Eq. (1) because considerable cancelation often exists between them. Thus, as highlighted by Hoskins et al. (1978), the effect of each term in isolation could be misleading when attempting to diagnose the magnitude and even the sign of the vertical velocity.

To overcome this drawback, Trenberth (1978) proposed an alternative but complementary approach, suggesting that upward motion is present in the mid-troposphere where there is advection of cyclonic vorticity by the thermal wind. Hoskins et al. (1978) developed a Q-vector approach for operational vertical motion estimation, in which the first two terms on the right-hand side of Eq. (1) are combined and the quasi- geostrophic forcing of vertical motion is written in a single term (the so-called divergence of the Q-vector), which means the cancelation problem is negated. This improved method, which is more exact than the approach proposed by Trenberth (Dunn, 1991), was used widely during subsequent years. However, it was found inconvenient in operational application because of the difficulty in determining the Q-vector directly from weather charts (Dunn, 1991). For this, Sanders and Hoskins (1990) proposed an easy method for estimation of the directions and relative magnitudes of Q-vectors from weather maps.

Considerable effort has also been concentrated on linking the upper-level PV anomaly or PV advection to vertical velocity in the lower troposphere (Hoskins et al., 1985; Thorpe, 1985; Waugh & Polvani, 2000; Funatsu & Waugh, 2007). Hoskins et al. (2003, HPJ03 hereafter)

made a breakthrough by formulating the link of vertical velocity with PV advection in z-coordinates. Based on the adiabatic thermodynamic equation, the vertical velocity of the adiabatic flow was partitioned into two components: the isentropic gliding (IG, hereafter) vertical velocity ( $w_{IG}$ ) and the isentropic displacement (ID, hereafter) vertical velocity ( $w_{ID}$ ). The $w_{IG}$ ( $w_{IG} = -N^{-2}(\overrightarrow{V_g} - \vec{C}) \cdot \nabla_h b$ , $b = g\theta / \theta_0$ , where $\theta_0$ is a constant potential temperature, $N = (g\theta_0^{-1}\Theta_z)^{1/2}$ is the basic state Brunt–Väisälä buoyancy frequency, $\Theta(z)$ and $\Theta_z$ are the same as $\Theta(p)$ and $\Theta_p$, respectively, except for p-coordinates, $\vec{C}$ is the horizontal velocity of a moving frame of reference, and $\nabla_h$ is the horizontal gradient operator) is associated with the horizontal motion of a particle moving along a sloping isentropic surface, whereas the $w_{ID}$ ( $w_{ID} = -N^{-2}(\partial b / \partial t)\big|_C$ ) measures the rate of vertical displacement of a particle that is associated with the development of the thermal field as well as the "development" of the system's circulation. It was further shown that the component of $w_{ID}$ satisfies a conventional omega equation but with forcing determined solely by the vertical gradient of quasi-geostrophic PV ( $q_g$ , QGPV hereafter) advection (Eq. 11 in HPJ03):

$$\begin{cases} [N^2\nabla_h^2 w_{ID} + f^2 \dfrac{\partial}{\partial z}(\dfrac{1}{\rho_r}\dfrac{\partial \rho_r w_{ID}}{\partial z})] = f\dfrac{\partial}{\partial z}[(\vec{V}_g - \vec{C}) \cdot \nabla_h q_g] \\ q_g = f + \nabla_h^2 \psi + \dfrac{f^2}{\rho_r}\dfrac{\partial}{\partial z}(\dfrac{\rho_r}{N^2}\dfrac{\partial \psi}{\partial z}) \\ \text{Boundary condition: } w_{ID} = N^{-2}(\overrightarrow{V_g} - \vec{C}) \cdot \nabla_h b \text{ on z = constant} \end{cases} . \quad (3a)$$

Where $\psi$ is the geostrophic stream function, $\rho_r$ the basic-state density. Therefore, the ID vertical velocity becomes a solely response to the interior redistribution of QGPV, i.e., increase of QGPV advection with increasing height will result in vertical air ascent ( $w_{ID} > 0$), and vice versa. The cancellation problem is negated, and the mechanism is concise and lucid.

The solution of $w_{ID}$ can be considered the sum of two parts: one associated with interior QGPV advection and the other associated with boundary temperature advection. In the presence of diabatic heating $H$ ($H(x, y, z)=db/dt$), a diabatic ID vertical velocity $w_{DID}$ that is identical to $w_{ID}$ and a diabatic IG vertical velocity $w_{DIG}$ ($w_{DIG} = -N^{-2}(\vec{V_g} - \vec{C}) \cdot \nabla_h b + N^{-2} H$) were defined. It was shown that the omega equation for $w_{DID}$ is the same as for $w_{ID}$ (Eq. 37 in HPJ03), and that the effect of heating on ID vertical velocity is present only implicitly in its impact on the tendencies of QGPV (Eq. 38a in HPJ03) and boundary temperature (Eq. 38b in HPJ03):

$$\begin{cases} [N^2 \nabla_h^2 w_{\mathrm{ID}} + f^2 \dfrac{\partial}{\partial z}(\dfrac{1}{\rho_r}\dfrac{\partial \rho_r w_{\mathrm{ID}}}{\partial z})] = -f \dfrac{\partial}{\partial z}\left.\dfrac{\partial q_g}{\partial t}\right|_C, \\ \left.\dfrac{\partial q_g}{\partial t}\right|_C = -(\vec{V_g} - \vec{C}) \cdot \nabla_h q_g + \dfrac{gf}{\theta_0 \rho_r}\dfrac{\partial}{\partial z}(\dfrac{\rho_r}{N^2} H) \\ \left.\dfrac{\partial b}{\partial t}\right|_C = -(\vec{V_g} - \vec{C}) \cdot \nabla_h b + H \quad \text{on horizontal boundary} \end{cases} . \qquad (3b)$$

Once the tendencies are expressed in terms of system-relative advection and heating as pointed out in HPJ03, the effects of heating on $w_{ID}$ will become explicit which will be performed in this study.

This novel omega equation developed by HPJ03 provides a tool for understanding how the interior redistribution of PV and boundary temperature advection can initiate vertical motion associated with system development. However, $w_{ID}$ is only a part of the full vertical velocity, and mere use of $w_{ID}$ to interpret the development of weather system may be misleading. Furthermore, all omega equations are diagnostic by nature, providing only the link between vertical velocity and the dynamic and thermodynamic conditions at a given time $t = t_0$. At $t_0$, the different components of vertical velocity ($w_{ID}$ ($t_0$) and $w_{IG}$ ($t_0$)) can be

calculated separately, albeit compensation or cancellation may exist as demonstrated in Figure 1 of HPJ03. However, during the development and evolution of a weather system ($t > t_0$), these different components can interact with each other as will be discussed below. Therefore, determining the approach for how best to employ the omega equation of $w_{ID}$ to interpret the evolution of a weather system becomes a challenge.

**1.2 Impact of mountains on downstream PV development**

PV theory has been used widely in dynamic analysis of weather systems, as reviewed in Hoskins et al. (1985). The celebrated hydrodynamic PV equation developed by Ertel (1942) is:

$$\begin{cases} \dfrac{dP}{dt} = \alpha[\vec{\zeta}_a \cdot \nabla\dot{\theta} + \nabla \times \vec{F} \cdot \nabla\theta] \\ P = \alpha\vec{\zeta}_a \cdot \nabla\theta \end{cases} \tag{4}$$

where $\alpha$ is specific volume, $\vec{\zeta}_a$ is 3D absolute vorticity, $\vec{F}$ is 3D frictional acceleration in the momentum equation, and $\nabla$ is a 3D gradient operator. The PV equation (4) considers the impact of both diabatic heating and friction; therefore, it is appropriate for application to an open dissipative system and suitable for climate studies.

During previous decades, the effect of near-surface PV generation on atmospheric circulation has attracted much attention. For example, Haynes and McIntyre (1987, 1990) and Schneider et al. (2003) introduced the concept of PV density (PVD, $W = \rho \cdot P = \vec{\zeta}_a \cdot \nabla\theta$, where $\rho = \alpha^{-1}$ is air density). They demonstrated that the total PV change along an isentropic surface intersecting the ground is determined by the integral of the normal component of PVD flux along the boundary where the isentropic surface intersects the ground surface in the part of the "underworld" defined by Hoskins (1991). The studies of Held and Schneider (1999), Koh and Plumb (2004), Schneider (2005), Egger et al. (2015), and others have also

demonstrated that the surface boundary PV can substantially influence interior atmospheric circulation. These studies have indicated that PV in the free atmosphere is linked closely to surface PV generation. However, the questions of how PV is generated at the ground surface and how the generated surface PV might be transferred into the interior of the atmosphere to influence the atmospheric circulation remain unclear and challenging.

One example is the formation of PV anomalies in the lee of high terrain, which has long been the subject of research directed toward understanding the influence of mountains on downstream weather and climate. In a study of PV change of airflow parallel to the Alps, Thorpe et al. (1993) found the Alps a significant source of PV anomalies in the lower troposphere, with negative and positive PV anomalies on the northern and southern sides of the Alps, respectively. Such anomalies, which are advected away from the orography, become an important part of the tropospheric PV budget. Using high-resolution numerical model simulations, Aebischer and Schär (1998) showed that when the direction of the synoptic-scale wind is perpendicular to the Alps, low-level elongated PV banners are generated downstream. Furthermore, individual pairs of banners with anomalously positive and negative PV values can be attributed to flow splitting, either on the scale of the entire Alpine region or on that of individual massifs and peaks of the model topography. These banners evolve and grow when the orographically generated PV anomalies are advected downstream. In short, the PV of air flowing past high mountains can be altered and PV banners generated downstream of a complex mountain barrier can affect the downstream circulation and weather.

The Tibetan Plateau (TP), located in western China, covers an area of $2.5 \times 10^6$ km$^2$, i.e., approximately one quarter of the entire land territory of China. It extends to elevations of >5 km above sea level. Many of the synoptic-scale systems that cause damaging floods in China have their origins in the region of the TP and its surroundings (Tao & Ding, 1981; Chen & Dell'osso, 1984; Yasunari & Miwa, 2006). Previous studies (Shi et al., 2000; Wang et al.,

2008; Zheng et al., 2013; Wang et al., 2014; Ma et al., 2020) have focused primarily on the influence of the TP on severe weather events during summer due to its unique thermodynamic forcing (Yeh et al., 1957; Ding et al., 1994; Chen et al., 1996; Wu et al., 1997, 2007, 2017; Li et al., 2002; Li et al., 2016; Liu et al., 2020). In winter, a strong westerly flow that dominates the subtropical troposphere over Asia is split into northern and southern branches in the lower troposphere when it impinges the western TP (Yeh, 1950). Over the eastern TP, near-surface airflows with different origins converge from the north and the south, resulting in circulation perturbations that are then advected eastward by the westerly winds (Wan & Wu, 2007; Li et al., 2011; Pan et al., 2013; Ma et al., 2019; Yu et al., 2019). Similar to the Alps, circulation change in the region of the TP could act as a significant source of PV anomalies in the lower troposphere and generate downstream PV perturbations. The Yangtze River Basin, which is located downstream of the TP, is one area in China that frequently receives heavy precipitation associated with weather system development irrespective of season. However, the mechanism via which weather system development in winter might be related to PV generation in the lee of the TP remains unclear and constitutes another research challenge.

In this study, we employ a case diagnosis to elucidate how a winter weather system developed downstream of the TP in the diabatic atmosphere from the perspective of PV and the omega equation in p-coordinates. Two datasets are used for the diagnosis: 6-h cumulative precipitation data from 629 rain gauge stations distributed across China, obtained from the China Meteorological Administration (https://data.cma.cn/data/cdcdetail/dataCode/SURF_CLI_CHN_MUL_DAY_V3.0.html), and MERRA-2 data produced by the Global Modeling and Assimilation Office (Gelaro et al., 2017) based on the terrain-following hybrid σ-p coordinates of the GEOS-5 model. Three collections of MERRA-2 data are used: the basic assimilated meteorological fields on both

pressure levels and model levels, and atmospheric state variables at the surface level provided on a 0.625° × 0.5° (longitude × latitude) grid and sampled at 3-h intervals.

The remainder of the paper is arranged as follows. Section 2 introduces the circulation background of the selected weather event and analyzes the PV restructuring of the airflow passing the TP as well as the evolution of the related circulation. Section 3 presents descriptions of both the evolution of PV advection downstream of the TP and the triggering of cyclogenesis and vertical velocity by focusing on adiabatic processes. The interaction between the ID vertical velocity and the IG vertical velocity is also explored. Section 4 provides a PV–Q perspective on vertical velocity development, including the interaction between the IG vertical velocity and the vertical velocity induced by diabatic heating Q, as well as the feedback of heating on PV forcing and the ID vertical velocity. The evolution of cyclogenesis associated with meridional and zonal PV advection is analyzed in Section 5. Conclusions are provided in Section 6.

## 2. Background of the weather event and PV evolution downstream of the TP

### 2.1 Circulation background of the weather event

In January and early February 2008, southern China, including the Yangtze River Basin, experienced extreme and persistent low temperatures and severe freezing precipitation just before the Chinese Spring Festival. Detailed analysis of the synoptic-scale process (Tao & Wei, 2008) indicates that the freezing precipitation occurred because of the existence of an inversion layer in the lower troposphere in Southern China as is commonly observed in the season; and that this event resulted from the combined effects of multiple factors, which included the western Pacific subtropical high in the lower troposphere, a quasi-stationary front over southern China, and the eastward propagation of a cold trough from central Asia across the TP in the mid-troposphere. However, the mechanism via which such an extreme weather event might be linked to the forcing of the TP remains unclear. Thus, a synoptic

episode that occurred during 17–21 January 2008 is selected for diagnosis from the perspective of PV and the omega equation. During this period, the observed maximum daily precipitation amount, including freezing rain and snow, exceeded 30 mm in some areas (Shi et al., 2008, also refer to Fig. 1i), causing severe damage to local transportation, electrical power lines, and agriculture.

Figure 1 presents the evolution of the daily tropospheric circulation and precipitation over central and eastern China during 17–19 January 2008. At 500 hPa, westerly flow swept over the TP and East Asia. No remarkable perturbation was observed in the subtropics on 17 January (Fig. 1a). However, on the following day, a center of weak positive vorticity appeared over southwestern China (Fig. 1b), which became enhanced and expanded eastward (Fig. 1c). At 650 hPa, a center of high relative vorticity appeared first over the eastern flank of the TP on 17 January (Fig. 1d). It intensified gradually and then spread eastward during the following two days (Fig. 1e and 1f). Coincident with the intensification of the center of relative vorticity, a trough developed to the east of the TP on 18 January, which became strengthened on 19 January. The center of relative vorticity at 850 hPa was located along the Yangtze River Basin (~30°N) and to the east of the corresponding relative vorticity center at 650 hPa (Fig. 1g–i), which enhanced gradually during 18–19 January over southern China. The distribution of the atmospheric circulation in the mid- and lower troposphere favored development of ascending air and precipitation. Organized large-scale precipitation started to develop on 18 January over South China (Fig. 1h), which increased considerably as it moved eastward during the following day (Fig. 1i). The observed maximum daily precipitation over the Yangtze River Basin (28°–34°N, 113°–121°E; box area R in Fig. 1i) on 19 January exceeded 10 mm and it was as high as 20 mm in some areas.

Figure 2 presents the evolution during 17–18 January 2008 and along 33°N of the longitude–height distributions of Ertel PV, circulation (u, $-\omega$), and potential temperature ($\theta$).

A striking feature in the configuration of the isentropic surfaces is their eastwardly dispersed distribution, i.e., from west to east, the isentropic surfaces tilt upward in the middle and upper troposphere but downward in the lower troposphere. This is because a strong cold trough known as the Northeast Asia Grand Trough exists in the upper troposphere over Northeast Asia in winter. Severe cold air is transported steadily southward by the northerly wind associated with the cold trough to East China, where the temperature in the free atmosphere is very low. The isentropic surfaces in the upper troposphere thus slope upward. Conversely, in the lower troposphere, the cold land surface to the west and the warm ocean surface to the east cause the isentropic surfaces to slope downward. Consequently, static stability decreases eastward downstream of the TP. This climatic feature is common in winter over East China. When adiabatic airflow propagates eastward downstream of the TP under the climatic background of decreasing static stability, its vertical vorticity is easily increased. This result at least partly explains the increase of the center of relative vorticity at 650 hPa during its eastward movement from the eastern flank of the TP on 17 January to eastern China on 19 January (Fig. 1d–f).

In Fig. 2, it is shown that the atmosphere over the region east of 110°E was characterized by dominant air descent and strong cooling on early 17 January, but that this changed to dominant air ascent and strong heating on 18 January. This feature is associated with the generation and eastward propagation of high PV over the eastern flank of the TP. At 06 UTC (Fig. 2b) of 17 January, a center of high PV (>1.5 PVU) appeared on the surface over the eastern flank of the TP with weak air ascent nearby to its east. Subsequently, the center of high PV extended eastward gradually; by 00 UTC on 18 January (Fig. 2e), the forefront of the 1.5 PVU contour had already passed 110°E and air ascent developed over eastern China, implying a potential link of vertical velocity development to PV advection.

**2.2 PV restructuring in the region of the TP**

The PV equation (Eq. 4) indicates that external forcing, i.e., either diabatic heating or frictional dissipation, can change the atmospheric circulation. Even in adiabatic and frictionless circumstances in which PV is conserved, the circulation can still change via internal conversion among, or "restructuring" of, the different PV components, i.e., the 3D absolute vorticity ($\vec{\zeta}_a$), static stability ($\partial\theta/\partial z$), baroclinicity ($\partial\theta/\partial x, \partial\theta/\partial y$), and specific volume ($\alpha$) associated with convergence. The highly elevated TP intersects the isobaric and isentropic surfaces in the mid- and lower troposphere. The airflow in the lower troposphere that is split by the TP converges near the surface in the lee of the TP, resulting in a circulation anomaly due to changes in the PV structure that accompanies surface convergence. The downstream westerly flow might experience further change in PV structure associated with static stability variation. Such a process of PV restructuring induced by TP forcing could have considerable effects on the ambient atmospheric circulation, its thermal structure, and downstream weather development. Here via diagnosing the above selected cyclogenesis event, we analyze how the PV structure of the airflow changes in the region of the TP and how subsequent advection of PV downstream of the TP affects the development of the weather system and its vertical motion.

The system of interest is the relative vorticity center initially located over the eastern TP at 650 hPa, which subsequently propagated eastward and intensified over the Yangtze River Basin (Fig. 1d–f). Unlike the PV banner in the lee of Alps which usually possesses pairs of anomalously positive and negative PV values, the relative vorticity center over the eastern TP presents as a positive sheet. Its formation is related to PV restructuring within the boundary layer in the region of the TP. To demonstrate this, the PV is partitioned into two components:

$$P = \alpha W,$$

in which $W=\vec{\zeta}_a \cdot \nabla\theta$ is the amount of PV per unit volume, i.e., PV density $W$ (Haynes & McIntyre, 1987, 1990; Schneider et al., 2003). From the PV equation (4), the PVD equation

can be obtained:

$$\frac{dW}{dt} = \alpha^{-1}\left(\frac{dP}{dt} - W\frac{d\alpha}{dt}\right) = -W\nabla\cdot\vec{V} + \vec{\zeta}_a\cdot\nabla\dot{\theta} + \nabla\times\vec{F}\cdot\nabla\theta\,. \quad (5)$$

It implies that in addition to diabatic heating and friction, convergence of airflow associated with the change in specific volume can also cause a change in *W*. In terrain-following hybrid σ-p coordinate

$$\sigma = (p - p_T)/(p_S - p_T)\,,$$

the local change of $W_\sigma$ becomes

$$\underset{(I)}{\frac{\partial W_\sigma}{\partial t}} = -\nabla_\sigma\cdot[\underset{(II)}{\vec{V}W_\sigma} - \underset{(III)}{\vec{\zeta}_{a\sigma}\dot{\theta} - \theta\nabla_\sigma\times\vec{F}_\sigma}]\,, \quad (6)$$

in which $p_S$ is pressure at the ground surface (depending on elevation), $p_T$ is pressure at the top of the domain ( $p_T$ = 0.01 hPa in MERRA-2), subscript $\sigma$ denotes the variable in $\sigma$-coordinates, and the gradient operator $\nabla_\sigma = \frac{\partial}{\partial x}\vec{i} + \frac{\partial}{\partial y}\vec{j} + \frac{\partial}{\partial\sigma}\vec{k}$. Using the MERRA-2 terrain-following hybrid $\sigma$-p coordinate data, the influence of airflow convergence on PV restructuring in the surface boundary layer can be estimated, the results of which are presented in Fig. 3. The local change (Eq. (6) term I) and the contributions from both PVD flux convergence (term II) and diabatic heating (term III) are shown in the first, second, and third columns, respectively. For attribution purposes, the contribution from air convergence ($-W_\sigma\nabla_\sigma\cdot\vec{V}$) which is one component of term II is also shown in the right column. During this period, two notable centers of positive PVD tendency appear over the eastern TP south of 35°N. The southern center, which is located near 26°N with elevation just above 1.5 km, is associated with a stationary cold front over southern China. The northern center, located around 33°N with elevation of 3–4 km (first column), aligns well with the position of the

positive vorticity center at 650 hPa shown in Fig. 1d. The formation of these two centers is largely due to PVD flux convergence (second column), whilst the contribution from diabatic heating is small (third column). Partitioning the W flux convergence into two components shows that the contribution from air convergence ($-W_\sigma \nabla_\sigma \cdot \vec{V}$) is dominant (right column), whereas the component associated with the advection of W ($-\vec{V} \cdot \nabla_\sigma W_\sigma$) is small, particularly over the eastern flank of the TP (figures not shown). These results indicate that mainly due to the conversion between specific volume α and PV density *W*, the near-surface convergence of airflow in the region of the TP contributes to the increase of PVD over the eastern flank of the TP.

**2.3 Evolution of circulation and vorticity**

Figure 4 presents the evolutions during 17–20 January 2008 of the relative vorticity (purple curve) averaged over box area V (28°–34°N, 105°–113°E, Fig. 1f) at 650 hPa, together with the precipitation (black curve), vertical velocity at 650 hPa (red curve), and vertical integral of convergence of water vapor flux from the surface to 650 hPa (blue curve) averaged over box area R (28°–34°N, 113°–121°E, Fig. 1i) which is located downstream of box area V. The evolution of the relative vorticity can be separated into four stages: I, Initial Stage (12 UTC 17 January to 00 UTC 18 January); II, Developing Stage (00 UTC 18 January to 00 UTC 19 January); III, Maturation Stage (00 UTC 19 January to 00 UTC 20 January); and IV, Decaying Stage (00 UTC 20 January to 18 UTC 20 January). In Stage I, relative vorticity was triggered to the east of the TP by 12 UTC on 17 January, followed by downstream development of air ascent and lower-layer convergence of water vapor flux, but with no appreciable precipitation (Fig. 1g). During Stage II, as rapid development of cyclonic vorticity occurred in area V, air ascent and lower-layer water vapor convergence in the downstream area R intensified quickly with remarkable increase of precipitation (Fig. 1e and 1h). The intensity of the relative vorticity in area V and the precipitation in area R reached

their maxima in Stage III (Fig. 1f and 1i), before decaying quickly in Stage IV (Fig. 4). The other elements exhibited similar trends, except the decay of vertical velocity and the lower-layer convergence happened earlier and faster. These results imply that the system development represented by the evolution of relative vorticity at 650 hPa is fundamental in controlling the evolution of the entire weather process, including the vertical motion and the precipitation.

## 3. PV advection and triggering of vertical velocity and cyclogenesis

The seminal work of HPJ03 reveals a dynamic link of $\omega_{\mathrm{ID}}$ with PV advection. However, $\omega_{\mathrm{ID}}$ is only a small part of the full vertical velocity, whereas the PV advection or redistribution can lead to the development of full vertical velocity and cyclogenesis (Hoskins et al., 1985). How the triggering of $\omega_{\mathrm{ID}}$ contributes to the development of full vertical velocity and cyclogenesis is unclear and will be explored here firstly **for adiabatic circumstance**.

### 3.1 Triggering of $\omega_{\mathrm{ID}}$, $\omega_{\mathrm{IG}}$ and cyclogenesis

The link between the perspectives of the quasi-geostrophic omega equation and PV in p-coordinates for a diabatic atmosphere can be obtained by following the approach of HPJ03 in z-coordinates for an adiabatic atmosphere. For a frame of reference moving at constant horizontal velocity $\vec{C}$, the QGPV and thermodynamic equations can be written, respectively, as follows:

$$[\frac{\partial}{\partial \mathrm{t}}\Big|_C + (\vec{V}_g - \vec{C})\cdot\nabla]q_g = f\frac{\partial}{\partial p}(\frac{\dot{\theta}}{\Theta_p}) \tag{7}$$

and

$$[\frac{\partial}{\partial \mathrm{t}}\Big|_C + (\vec{V}_g - \vec{C})\cdot\nabla]\theta = -\Theta_p\omega + \dot{\theta}. \tag{8}$$

In the above, the QGPV is defined as

$$q_g = f + f^{-1}\nabla_h^2\Phi + f\frac{\partial}{\partial p}\left(\frac{1}{\Sigma^2}\frac{\partial\Phi}{\partial p}\right) = f + f^{-1}\nabla_h^2\Phi + f\frac{\partial}{\partial p}\left(\frac{\theta}{\Theta_p}\right), \tag{9}$$

where the hydrostatic relation is $\partial\Phi/\partial p = -\Pi(p)\cdot\theta$. From Eq. (8), the vertical velocity of diabatic flow ($\omega$) can be divided into three components, i.e., the $\omega_{\mathrm{ID}}$, $\omega_{\mathrm{IG}}$, and the diabatic heating vertical velocity ($\omega_{\mathrm{Q}}$):

$$\omega = \omega_{\mathrm{ID}} + \omega_{\mathrm{IG}} + \omega_{\mathrm{Q}}, \tag{10}$$

with

$$\omega_{\mathrm{ID}} = -\Theta_{\mathrm{p}}^{-1}\left(\frac{\partial\theta}{\partial \mathrm{t}}\right)\Big|_{\mathrm{C}}, \tag{11}$$

$$\omega_{\mathrm{IG}} = -\Theta_{\mathrm{p}}^{-1}(\overrightarrow{\mathrm{V}_{\mathrm{g}}} - \vec{\mathrm{C}})\cdot\nabla\theta, \tag{12}$$

and

$$\omega_{\mathrm{Q}} = \Theta_{\mathrm{p}}^{-1}\dot{\theta}. \tag{13}$$

The implication of $\omega_{\mathrm{ID}}$ and $\omega_{\mathrm{IG}}$ is the same as what is defined in HPJ03 and interpreted in Section 1.1, whereas the $\omega_{\mathrm{Q}}$ term is related to diabatic heating. For a diabatic atmosphere, the $\omega_{\mathrm{ID}}$ is equivalent to $w_{DID}$ in HPJ03, whilst the sum of $\omega_{\mathrm{IG}}$ and $\omega_{\mathrm{Q}}$ is equivalent to their $w_{DIG}$. The separation of $\omega_{\mathrm{Q}}$ from $\omega_{\mathrm{IG}}$ is for the use of following diagnosis. From Eqs. (7) to (11), the omega equation for $\omega_{\mathrm{ID}}$ in a diabatic atmosphere can be obtained (Appendix):

$$\begin{cases} \mathrm{L}\{\omega_{\mathrm{ID}}\} = [\Sigma^2\nabla_h^2 + f^2\dfrac{\partial^2}{\partial p^2}]\,\omega_{\mathrm{ID}} = f\dfrac{\partial}{\partial p}[(\vec{V}_g - \vec{\mathrm{C}})\cdot\nabla q_g] - f^2\dfrac{\partial^2}{\partial p^2}\left(\dfrac{\dot{\theta}}{\Theta_p}\right) \\ \qquad\qquad = F_1 + F_2 = F, \\ \text{in which } F_1 = f\dfrac{\partial}{\partial p}[(\vec{V}_g - \vec{\mathrm{C}})\cdot\nabla q_g],\ \ F_2 = -f^2\dfrac{\partial^2}{\partial p^2}\left(\dfrac{\dot{\theta}}{\Theta_p}\right), \\ \omega_{\mathrm{ID}} = \Theta_p^{-1}(\overrightarrow{V_g} - \vec{C})\cdot\nabla\theta - \Theta_p^{-1}\dot{\theta}, \qquad \text{on horizontal boundary.} \end{cases} \tag{14}$$

In a diabatic case ($Q = \dot{\theta} \neq 0$), Eq. (14) is equivalent to Eq. (3b) for $w_{DID}$. Heating can induce extra local change in potential temperature (Eq. (8)) and it can change $\omega_{ID}$ (Eq. (11)). In an adiabatic case ($\dot{\theta} = 0$ and $F_2$=0), Eq. (14) is equivalent to Eq. (3a) for $w_{ID}$. For the weather episode of current case study, the forefront of the 1.5 PVU contour propagates eastward from 107°E on 06 UTC 17 January (Fig. 2b) to 112°E on 18 UTC 18 January (Fig. 2h) with speed $|\vec{C}|$ (< 4 m s$^{-1}$) that is much slower than the basic flow $|\vec{V}_g|$ (which is close to $|\vec{V}|$ (~10-20 m s$^{-1}$), as shown in Fig. 2), i.e., $\vec{V}_g - \vec{C} \approx \vec{V}_g$. Therefore, according to Eq. (14), ID air ascent ($\omega_{ID}$ < 0) is generated when QGPV advection increases with height, and vice versa.

Eq. (14) is only a diagnostic equation for a given time t=$t_0$. A natural extension of the above conclusion is how the initiation of $\omega_{ID}$ leads to the triggering of $\omega_{IG}$ and cyclogenesis afterwards (t>$t_0$). Let the characteristic horizontal and vertical scales of the system under consideration be $L$ and $H$ ($\approx P_0/\rho_0 g$, where $P_0$ is the characteristic pressure depth and $\rho_0$ is the characteristic density), respectively. Then, the ratio between the first and second terms on the left-hand side of Eq. (14) becomes $R = (NH / fL)^2$. For adiabatic large-scale motion in which $L >> NH/f$, the second term on the left-hand side of Eq. (14) is much larger than the first. Thus, Eq. (14) can be qualitatively approximated to the following:

$$f^2 \frac{\partial^2 \omega_{ID}}{\partial p^2} \approx -f \frac{\partial}{\partial p}\left(\frac{\partial q_g}{\partial t}\bigg|_C\right) = f \frac{\partial}{\partial p}[(\vec{V}_g - \vec{C}) \cdot \nabla q_g].$$

Thus,

$$f \frac{\partial \omega_{ID}}{\partial p} \approx -\frac{\partial q_g}{\partial t}\bigg|_C = [(\vec{V}_g - \vec{C}) \cdot \nabla q_g]$$

and

$$\left.\frac{d\zeta_g}{dt}\right|_{\mathrm{ID}} \propto f\frac{\partial\omega_{\mathrm{ID}}}{\partial p} = -f\nabla_{\mathrm{h}}\cdot\vec{V}_{ID} \approx [(\vec{V}_g - \vec{\mathrm{C}})\cdot\nabla q_g]\,. \tag{15}$$

For an adiabatic case, Eq. (15) indicates that positive QGPV advection causes horizontal divergence, whereas negative QGPV advection causes horizontal convergence and development of cyclonic relative vorticity. Thus, a configuration with negative PV advection below and positive PV advection aloft, that is an increase of PV advection with increasing height, will lead to cyclogenesis in the lower layer and ascending $\omega_{\mathrm{ID}}$ in between owing to the atmospheric continuity. Furthermore, the convergence flow ($\vec{V}_{ID}$) in the lower layer induced by the negative PV advection should move along the isentropic surfaces, forcing the IG flow ($\vec{V}_{IG} \equiv \vec{V}_{ID}$). According to (12), IG vertical velocity is upward ($\omega_{IG} < 0$) when the flow $\vec{V}_{IG}$ is along positively sloped isentropic surface and downward when it is along negatively slopped isentropic surface. For a stably stratified atmosphere, isentropic surface always tilts upward towards cold area, adiabatic air flow $\vec{V}_{IG}$ towards cold area (or warm advection) should ascend while descend if it is towards warm area (or cold advection). For the winter weather event under investigation, as the isentropic surfaces in the lower troposphere tilt upward toward the north, the development of southerly flow to the east of a center of cyclogenesis will result in associated IG air ascent:

$$(\omega_{\mathrm{IG}})_v = -v_{IG}(\partial\theta/\partial y)\Theta_p^{-1} < 0\,. \tag{16}$$

At the same time, the isentropic surfaces in the lower troposphere over East Asia tilt downward toward the east (Fig. 2), the convergence ($\nabla_{\mathrm{h}}\cdot\vec{V}_{IG} < 0$) in the lower layer will also result in IG ascending easterlies:

$$(\omega_{\mathrm{IG}})_u = -u_{IG}(\partial\theta/\partial x)\Theta_p^{-1} < 0\,. \tag{17}$$

Consequently, ascending IG vertical velocity ($\omega_{IG} < 0$) and cyclogenesis are triggered in the lower layers by the development of $\omega_{ID}$ aloft due to the sloping of isentropic surfaces, i.e.,

the baroclinicity of the atmosphere: the stronger the baroclinicity, the stronger the ascending $\omega_{IG}$.

On the steep eastern flank of the TP, many isobaric surfaces intersect the surface of the TP. The PV generated near the surface at these locations (Figs. 2 and 3) can be advected toward downstream areas and thus influence the in situ circulation. Figure 5 shows the evolutions of PV at 650 hPa, $\omega_{\mathrm{ID}}$ at 700 hPa, and relative vorticity ($\zeta$), potential temperature ($\theta$), $\omega_{\mathrm{IG}}$, and streamlines at 850 hPa. To maintain consistency with Fig. 2, Ertel PV is used for constructing the panels in the left column in Fig. 5. This will not affect evaluation of the impact of QGPV advection because (to the first-order approximation) Ertel PV (*P)* and QGPV ($q_g$) satisfy the relation $q_g \approx P/[-g\Theta_p(p)]$ (Nielsen-Gammon & Gold, 2006).

In Stage I (Fig. 5a–c) there was no precipitation. According to Eqs. (14) – (17), PV advection at 650 hPa triggers the ascending $\omega_{\mathrm{ID}}$ at 700 hPa (Fig. 5a) and $\omega_{\mathrm{IG}}$ at the lower level of 850 hPa (Fig. 5b). The induced southerly (Fig. 5c) is associated with negative PV advection, which causes air convergence and the formation of cyclonic relative vorticity in situ (Eq. (15)). In a moving frame of reference with its origin located at the forefront of the 1.5 PVU contour of the high PV region over the eastern TP, significant ascending $\omega_{\mathrm{ID}}$ appears only close to the forefront (Fig. 5a), whereas strong ascending $\omega_{\mathrm{IG}}$ dominates the vertical motion away from the forefront (Fig. 5b). This is in good correspondence with the analytical result of an idealized case experiment of HPJ03 in which a prescribed constant QGPV is located at a height where the zonal wind speed is a constant westerly (refer to their Eq. 15 and Fig. 2). From Stage II to Stage III (Fig. 5d–i), as eastward PV advection at 650 hPa intensified (Fig. 5d and 5g), the cyclonic relative vorticity at 850 hPa and the associated ascending $\omega_{\mathrm{IG}}$ (Fig. 5e and 5h), together with the southerly flow to the east of the cyclone center (Fig. 5f and 5i), develop further. The warm advection and negative PV advection to the

east of the center become apparent, contributing to the slow eastward movement of the cyclone center (Eq. (15)). The entire process is similar to the schematic of cyclogenesis associated with the arrival of an upper-air PV anomaly over a lower-level baroclinic region (Hoskins et al., 1985). In Stage IV (Fig. 5j–l), as positive PV was advected rapidly to the western Pacific, the main cyclonic center moved from the continent to the Sea of Japan, the prevailing flow at 850 hPa over eastern China changed from southerly to northerly (Fig. 5l), and, following formula (16), the $\omega_{IG}$ changed from ascent to descent (Fig. 5k); consequently, the cyclonic vorticity decayed.

### 3.2 Evolution of different $\omega$ components

For a specific location (x, y, p), the $\omega_{ID}$, $\omega_{IG}$, and $\omega_{Q}$ at a given time ($t=t_0$) can be calculated separately from Eqs. (11-13). They may compensate or cancel to each other and their sum satisfies Eq. (10). However, the results from Fig. 5 demonstrate that during the cyclone evolution ($t>t_0$), they can influence each other. To reveal how the different omega components interact, the evolutions of $\omega_{ID}$, $\omega_{Q}$, and total $\omega$ at 700 hPa, together with the $\omega_{IG}$ and horizontal wind divergence at 850 hPa, are shown in Fig. 6. In Stage I when there was no precipitation, $\omega_{Q}$ was weak and descending. $\omega_{IG}$ was weak ascending because of the background southerly wind associated with the depression to the east of the TP (Fig. 1g). Owing to PV forcing, ascending $\omega_{ID}$ at 700 hPa was triggered by 06 UTC on 17 January. Consequently, ascending $\omega_{IG}$ at 850 hPa increased, leading to increasing vertical stretching and contributing to the development of the cyclonic vorticity and the southerly flow (Figs. 4 and 5c). The negative feedback of the $\omega_{IG}$ development on $\omega_{ID}$ as will be discussed caused the latter to start to weaken after 18 UTC on 17 January.

In Stage II, ascending $\omega_{IG}$ increased continuously, and ascending heating velocity $\omega_{Q}$ started to develop as $\omega_{ID}$ changed to descending. It is interesting to see that the intensity of

$\omega_{IG}$ started to decline at 18 UTC on 18 January before the vorticity and precipitation reached their peaks at 06 UTC on 19 January (Fig. 4). This is because the occurrence of precipitation along the Yangtze River Basin increases the in situ potential temperature and reduces the meridional gradient of potential temperature to its south. According to Eq. (16), the $\omega_{IG}$ should be weakened. Despite this, wind convergence at 850 hPa continued to increase and reached its maximum at 00 UTC on 19 January, i.e., at the beginning of Stage III, as did both the convergence of water vapor flux and the air ascent in the precipitation region of area R (Fig. 4). Six hours later, the total vertical air ascent $\omega$ at 700 hPa, cyclonic vorticity, and precipitation all reached their maxima (Figs. 4 and 6). As the $\omega_{IG}$ continued to weaken and changed from ascent to descent, water vapor supply was reduced and the ascending $\omega_{Q}$ also weakened. The ascending $\omega_{IG}$ presents throughout Stage I, II, and most of Stage III, and is much stronger than $\omega_{ID}$. This is similar to the theoretical results of HPJ03 (their Eq. 15) that the prominent quasi- geostrophic vertical motion can be mainly attributed to isentropic upgliding measured in a frame of reference moving with a speed close to the basic flow. In Stage IV, both $\omega_{IG}$ and $\omega_{Q}$ became positive, precipitation was weak, and $\omega_{ID}$ returned to ascent. The evolution of different omega components thus demonstrates that different omega components can interact with each other during system evolution and the diabatic heating and the associated $\omega_{Q}$ have strong impacts on both $\omega_{ID}$ and $\omega_{IG}$.

**3.3 Interaction between $\omega_{ID}$ and $\omega_{IG}$**

The eastward advection of high PV, which was generated over the eastern flank of the TP, triggered ascending $\omega_{ID}$ from below, with air convergence and cyclonic vorticity generation in the lower troposphere (Figs. 7a, 5a, and 5b). For adiabatic atmospheric motion, the converging southeasterly flow in the lower troposphere (Fig. 5c) should move along the isentropic surfaces ($\vec{V}_{IG} \equiv \vec{V}_{ID}$) and thus the upward IG flow ($\omega_{IG}$ <0) is generated as shown

in Fig. 5b and Fig. 6, and indicated by the solid brown arrow between Fig. 7a and 7b. It is important to note that $\omega_{ID}$ is ascending over southern China only in Stage I (Fig. 5a) and that it changes to descending afterwards (Fig. 5d and 5g). From Stage I to Stage II, the ascending southerly ( $v_{IG} > 0$, $\omega_{IG} < 0$, Eq. (16)) develops quickly (Fig. 5e and 5f). It transports warm moist air northward from the ocean to the Yangtze River region (Fig. 5f), causing the increase of local potential temperature that results in descending $\omega_{ID}$ (Eq. (11), Fig. 5d). Therefore, $\omega_{ID}$ receives a negative feedback from the development of $\omega_{IG}$ via warm advection as indicated by the dashed brown arrow ( $-\nabla\cdot(\vec{V}\theta)^{-}$ ) between Fig. 7b and 7a, leading to the weakening of $\omega_{ID}$ (Fig. 5a and 5d).

## 4. PV–Q perspective on vertical velocity development

The converging southeasterly flow associated with the ascending IG vertical velocity ( $\omega_{IG}$ <0) transported abundant water vapor from the ocean to South China and lifted the moist air upward (Fig. 7c and 5f). When the moist air reached the condensation level, precipitation started. The released latent heat (Q) associated with precipitation and condensation will affect the in situ PV (Eq. 7) as well as vertical velocity (Eq. 14). The evolution of vertical velocity **in the diabatic atmosphere** thus needs to be investigated from a PV-Q perspective.

### 4.1 Interaction between $\omega_{Q}$ and $\omega_{IG}$

Once the latent heat is released ( $\dot{\theta} > 0$), following the definition (13) air ascent associated with diabatic heating ( $\omega_{Q} < 0$) is generated. The development of ascending $\omega_{Q}$ intensifies the convergence and cyclonic circulation in the lower layers, and a stronger southerly wind together with enhanced $\omega_{IG}$ develops to the east of the cyclone center (Fig. 5e, 5f, 5h, and 5i). Thereby $\omega_{IG}$ gets positive feedback from the development of $\omega_{Q}$, as shown by the part of dashed brown arrow ( $-\nabla\cdot(\vec{V})^{+}$ ) between Fig. 7b and 7c. The southerly

wind produces not only warm advection but also negative PV advection in the lower layers (solid brown arrow ($\vec{Vq}$, $\vec{VP}$) between Fig. 7b and 7c). This is coupled with the arrival of high PV from the west in the upper layer (Fig. 5d and 5g), which leads to baroclinic cyclonic development to the east of the cyclone center and increases the local precipitation and diabatic air ascent ($\omega_Q < 0$), presenting a positive feedback between $\omega_{IG}$ and $\omega_Q$. Conversely, latent heating associated with precipitation increases the local potential temperature and reduces the meridional temperature gradient to its south, resulting in weakening of the ascending $\omega_{IG}$ (Eq. (16)). As shown in Fig. 6, the ascending $\omega_{IG}$ started weakening at 18 UTC on 18 January when the precipitation over the lower reaches of the Yangtze River Basin developed most rapidly (Fig. 1h and 1i). It indicates that $\omega_{IG}$ also receives a negative feedback from the development of $\omega_Q$ via reducing the upwind gradient of potential temperature (Fig. 7, the part of dashed brown arrow $\nabla\theta^-$ between Fig. 7b and 7c). Subsequently, the local $\omega_{IG}$ declined (Fig. 6), and both the water vapor flux convergence and the vertical velocity in this area started to decrease as well (Fig. 4). When $\omega_{IG}$ changed to descent late on the 19 January (Fig.5k and Fig. 6), the intensity of the cyclonic vorticity started to decay (Fig. 6) followed by weakening of the precipitation.

**4.2 Feedback of heating on PV forcing and $\omega_{ID}$**

It is interesting to see that $\omega_{ID}$ changed its sign after the precipitation occurred (Fig. 5 and Fig. 6), whilst the positive zonal PV advection at 650 hPa remained strong (Fig. 5, left column), which implies that diabatic condensation heating associated with precipitation must play a significant role in the evolution of vertical velocity. To reveal how diabatic heating can feedback on PV forcing and $\omega_{ID}$, Equation (14) is employed.

The evolutions during the period 17–20 January of the different forcing terms, together with $\omega_{ID}$ at 650 hPa and at 30°N averaged over 113°–121°E, are evaluated using the

analysis data and the results are presented in Fig. 8. It demonstrates that the forcing $F_1$ associated with vertical differential PV advection developed rapidly in Stage I and continued to act as positive forcing on $\omega_{ID}$ during the subsequent stages until the end of the Stage IV. The forcing $F_2$ associated with diabatic heating was weak in Stage I but became strongly negative during Stages II and III after precipitation occurred. Owing to the compensation and interaction between $F_1$ and $F_2$, the total forcing ($F = F_1 + F_2$) and $\omega_{ID}$ were weak and even changed their signs during these periods. In Stage IV, precipitation was reduced and $F_2$ became very weak, and the total forcing and $\omega_{ID}$ were determined mainly by $F_1$. All these results demonstrate that the forcing induced by vertically differential PV advection ($F_1$) plays a significant role in the triggering, development, and decay of the cyclonic circulation, while the initiated precipitation exerts considerable feedback on the ID vertical motion and system development.

Diabatic heating can exert both negative and positive impacts on $\omega_{ID}$, as shown schematically by the red arrows in Fig. 7 between panel (c) and (a). According to Eq. (14), latent heat release can produce negative forcing on $\omega_{ID}$ ($F_2 < 0$). Actually, by following the definition of Eq. (11), heating increases the local potential temperature and results directly in descending $\omega_{ID}$ (Fig. 7, red dashed arrow between Fig. 7c and 7a), as demonstrated in Figs. 5d, 5g, 5j, and 8, and schematically illustrated in Fig. 10d and 10g of HPJ03 for an infinite atmosphere at rest. For an atmosphere at motion, heating can change the PV advection and affect $\omega_{ID}$. This is because, according to the QGPV equation (Eq. (7)), heating generates positive PV below and negative PV above the heating maximum (Fig. 7c). Thus, the zonal PV gradient in the upper layer between the positive PV generated over the eastern TP and the induced negative PV over the heating region is intensified, as is the meridional PV gradient to the south of the heating region in the lower layer. Consequently, the increase of PV advection

with height is intensified, forming positive forcing on $\omega_{ID}$ ($F_1 > 0$) during the precipitation period as indicated by the red solid arrow between Fig. 7c and 7a. The total forcing for $\omega_{ID}$ is determined by the combined effect of $F_1$ and $F_2$, and $\omega_{ID}$ can change its sign during precipitation. During Stage IV, diabatic heating and the associated forcing $F_2$ are reduced, and the feedback of heating on the forcing $F_1$ becomes weakened as well.

In summary, we can conclude that strong interaction exists among the three omega components, which can significantly influence the circulation development during its life cycle. Although the development of ascending ID omega is important in initiating IG omega and inducing diabatic heating omega, it receives strong feedback from diabatic heating and it can even change its sign, whilst the forcing of the vertical differential PV advection has good correspondence with the evolution of the circulation and associated precipitation.

## 5. Roles of zonal and meridional PV advection in cyclogenesis

The above results demonstrate that it is the forcing of vertical differential PV advection together with the feedback from diabatic heating that modulates the evolution of the circulation and associated precipitation. This section further discusses how different PV advection coupling between the upper and lower layers influences the evolution of the circulation and associated precipitation.

### 5.1 Initial Stage (I)

The evolution from 12 UTC on 17 January to 00 UTC on 18 January of the vertical cross sections averaged between 113°–121°E of PV, its zonal and meridional advection, as well as wind are shown in Fig. 9. At 12 UTC on 17 January, a center of weak positive zonal PV advection appeared between 700 and 500 hPa at around 30°N (Fig. 9a), in correspondence with the eastward advection of the high PV that originated from the eastern flank of the TP (Fig. 2c). As the TP-induced high PV became enhanced and moved further eastward (Fig. 2d

and 2e), positive zonal PV advection increased downstream along the middle and lower reaches of the Yangtze River Basin (Fig. 9c and 9e), and positive relative vorticity and a southerly wind (mainly $\omega_{IG}$) developed in the lower troposphere (Fig. 5a- c). Concurrently, in the lower layer (below 700 hPa), negative meridional PV advection, with its center located above 850 hPa, increased over southern China (Fig. 9a, 9c, and 9e) and precipitation began to develop over southwestern China (Fig. 1).

The geostrophic advection of QGPV and its association with the development of vertical velocity are presented in the right column of Fig. 9. While positive PV advection developed in the mid-troposphere, negative PV advection in the lower tropospheric layer intensified because of the development of the cyclonic circulation and its related southerly winds within that layer. Consequently, PV advection increased with height below 500 hPa at around 30°N, suggesting forcing for ascent (Fig. 9b, 9d, and 9f). This ascent favored the development of convergence within the lower troposphere and the enhancement of southerly wind to the south of 30°N, which enhanced the transport of moist air to the Yangtze River Basin (Fig. 5c).

The above analysis demonstrates that during Stage I, forcing for ascent was induced mainly by the positive eastward advection of mid-tropospheric high PV, generated near the surface at the eastern flank of the TP, and by the enhanced negative meridional PV advection in the lower troposphere. Owing to the enhanced vertical gradient of QGPV advection, ascending vertical velocity was diagnosed to the southeast of the TP and in situ precipitation was initiated.

**5.2 Developing Stage (II)**

With the development of precipitation, the influence of diabatic heating associated with latent heat release on both vertical velocity and PV advection should be taken into consideration. Here, the changes in atmospheric circulation in the developing stage are

diagnosed using the PV equation (Eq. (7)).

With the development of ascending airflow on the southern side of the center of high PV, the southerly wind was strengthened and negative meridional PV advection in the lower troposphere was enhanced (Fig. 9). Thus, large-scale circulation with positive horizontal PV advection in the mid-troposphere and negative horizontal PV advection in the lower troposphere formed to the south of 30°N (Figs. 5d- f, and 10a), which further reinforced the forcing for quasi-geostrophic ascent (Fig. 10c).

A center of prominent diabatic heating was located in the mid-troposphere near 30°N, which generated a positive (negative) PV tendency below (above) its maximum center (Fig. 10b). The negative PV tendency above the precipitation area enhanced and sustained strong zonal PV advection upstream of the precipitation area. The vertical differential QGPV advection was thus enhanced compared with prior times, leading to further intensification of the vertical velocity between 28°N and 30°N (Fig. 10c).

In summary, during Stage II, vertical velocity and its associated precipitation over the middle and lower reaches of the Yangtze River Basin were highly related to the evolution of PV advection in the lower and mid-troposphere. During this period, the feedback of diabatic condensational heating contributed to both the maintenance of the zonal PV gradient, by acting to erode mid-tropospheric PV downstream of the area of high PV generated on the eastern flank of the TP, and the maintenance of the meridional PV gradient to its south, by acting to create lower tropospheric PV. These processes provide enhanced quasi-geostrophic forcing that enhances the cyclogenesis in the lower troposphere and supports both the development of vertical velocity and the associated precipitation.

**5.3 Maturation and Decay Stages (III and IV)**

During Stage III, as ascent in association with the enhanced southerly flow over the Yangtze River Basin (Fig. 5f and 5i) developed (Fig. 10), the center of negative meridional

PV advection was located at a higher altitude and closer to the center of positive zonal PV advection. When the precipitation peaked at 06 UTC on 19 January, a center of slightly stronger negative meridional PV advection was located immediately below the center of positive zonal PV advection, which resulted in the maximum magnitude of the vertical differential QGPV advection, in addition to the lifting of the vertical velocity center compared with earlier times (Fig. 11a and 11b). Subsequently, the center of negative meridional PV advection tended to overlay the positive center of zonal PV advection (Fig. 11c). Owing to prominent cancelation between the positive zonal PV advection and the negative meridional PV advection (Fig. 11e), both the vertical differential PV advection and the vertical velocity weakened (Fig. 11d and 11f). Meanwhile, the southerly wind weakened correspondingly (Fig. 11f), which led to reduced poleward advection of water vapor toward southern China. Consequently, the negative effect of diabatic heating on PV generation in the mid-troposphere decreased (not shown), which reduced the zonal PV gradient between the positive PV center over the eastern flank of the TP and the precipitation center over eastern China. Finally, as the cyclonic circulation decayed, the heavy precipitation diminished rapidly (Fig. 4) and the extreme winter precipitation event ended.

## 6. Conclusions

This study conducts a brief review of the development of the omega equation and the application of PV theory to the study of the impacts of large-scale mountains on downstream weather development. Several relevant challenges are also identified. The omega equation for $\omega_{\mathrm{ID}}$ constructed by HPJ03 is highlighted. As this equation establishes the link between $\omega_{\mathrm{ID}}$ and vertically differential PV advection, and as vertically differential PV advection is closely related with weather system development, this omega equation should be applicable to interpretation of weather system development. However, $\omega_{\mathrm{ID}}$ is only one part of the total vertical velocity, and the corresponding omega equation is a diagnostic equation. Therefore,

how best to use this diagnostic equation to interpret the development of full vertical velocity and the evolution of weather system has become a challenge.

In the current study, this challenge has been tackled by applying the QGPV equation (Eq. 7), the thermodynamic equation (Eq. 8), and the established ID omega equation (Eq. 14) for a diabatic atmosphere to the development of a weather event that occurred downstream of the TP during 17–21 January 2008. During the evolution of this event, positive PV was first generated over the eastern flank of the TP, and its subsequent eastward advection triggered the development of vertical velocity below and the generation of cyclone vorticity in the lower troposphere. The total vertical velocity of diabatic flow $\omega$ is partitioned into three components (i.e., $\omega_{\mathrm{ID}}$, $\omega_{\mathrm{IG}}$, and $\omega_{\mathrm{Q}}$). Consideration of the interactions of these components, together with analysis of the influence of diabatic heating Q on PV forcing, allows the impacts of the TP on PV generation and downstream development of both vorticity and vertical velocity, as well as the feedback of heating on PV advection, to be elucidated. The main results can be summarized as follows.

It has been shown that the development of the cyclone system associated with severe weather downstream of the TP is strongly tied both to the restructuring of PV near the surface due to airflow convergence in the region of the TP and to the subsequent downstream advection of positive PV in the mid-troposphere. The dynamical processes associated with the evolution of the cyclone system are depicted schematically in Fig. 12.

In winter the westerly flow impinging upon the TP in the lower troposphere is split by the TP and it converges over its eastern flank, causing the increase in PV density $W$ and the development of positive relative vorticity in that location. Since in winter the static stability $\partial\theta/\partial z$ near the TP is larger than in areas further downstream, the relative vorticity of the flow is increased easily as the PV advection is eastward. This is because along the westerly jet the vertical wind shear ($\partial u/\partial z$, $\partial v/\partial z$) and the horizontal components of potential

vorticity are small so that $P \approx \alpha(f+\zeta)\cdot\partial\theta/\partial z$ is conserved in adiabatic and frictionless circumstances. Thus, the TP plays a role in modulating the PV structure and in amplifying the relative vorticity of the passing airflow.

The downstream growth of PV advection leads to cyclogenesis in the lower troposphere and development of vertical velocity. In the Initial Stage (ST I, Fig. 12), positive zonal PV advection increases in the mid-troposphere, resulting in the development of ascending ID vertical velocity ($\omega_{ID}$<0). This is accompanied by wind convergence due to atmospheric continuity and by an increase of in situ relative vorticity in the lower troposphere, where an isentropic southerly wind develops in association with ascending IG vertical velocity ($\omega_{IG}$ < 0). Consequently, moist air is transported from the south, and negative meridional PV advection is increased, which contribute to quasi-geostrophic forcing for air ascent and cyclogenesis in situ. Thus, weak precipitation is initiated over southwestern China (ST I, Fig. 12) and ascending diabatic heating vertical velocity ($\omega_{Q}$ < 0) is generated. In the Developing Stage (ST II, Fig. 12) over eastern China, the increasing negative meridional PV advection associated with the strengthening southerly wind in the lower troposphere enhances the vertical differential PV advection between the mid- and lower troposphere, leading to enhanced forcing for quasi-geostrophic ascent compared to prior times. Meanwhile, the negative (positive) PV anomaly induced by diabatic condensation heating in the mid- (lower) troposphere weakens (enhances) the local PV over the precipitation region. Consequently, the zonal PV gradient in the mid-troposphere between the positive PV center over the eastern TP and the precipitation center, as well as the meridional PV gradient in the lower troposphere to the south of the precipitation center, are both enhanced. This provides persistent and strong positive zonal PV advection in the mid-troposphere and negative meridional PV advection in the lower troposphere for the development of both cyclonic vorticity and ascending vertical velocity.

During the Maturation Stage (ST III, Fig. 12), as the altitude of the ascending southerly flow is increased, the center of negative meridional PV advection is lifted further. When it becomes located immediately below the center of positive zonal PV advection, both cyclonic vorticity and air ascent with precipitation reach their maxima. At subsequent times (Decay Stage; ST IV, Fig. 12), the negative meridional PV advection substantially cancels the positive zonal PV advection, and both the vertical differential PV advection and the ascending airflow are weakened. The negative (positive) PV generation above (below) the center of convective diabatic heating decreases correspondingly and the zonal (meridional) PV gradient in the mid- (lower) troposphere upstream of the precipitation area is weakened. Consequently, along the middle and lower reaches of the Yangtze River Basin, the vertically differential PV advection decreases, air ascent is weakened, and precipitation diminishes.

It can be summarized that the frequent occurrence of a center of high PV over the eastern flank of the TP in winter is due to the PV restructuring associated with in situ surface convergence, and the eastward advection in the mid-troposphere of positive PV can trigger vertical velocity development and cyclogenesis in the lower troposphere. The evolution of the cyclone life is related closely to the interaction of different components of vertical velocity. It is the vertically differential PV advection and the feedback of diabatic heating that control the development and decay of vertical velocity and the evolution of the lower layer cyclone, as well as the weather downstream of the TP.

Current study only analyzes the impacts of the interior QGPV advection on the development of vertical vorticity. Since the solution of Equation (14) is also determined by boundary conditions, revealing the impacts of boundary temperature advection and diabatic heating on vertical velocity development will help further understanding the underlying physics. In this study, only one winter case is diagnosed to elucidate the proposed PV-Q perspective. Further analyses of other weather events, particularly in summer, are required.

**Acknowledgments**

All datasets used in this paper are publicly available. We would like to thank the China Meteorological Administration for releasing the precipitation data (downloaded from https://data.cma.cn/data/cdcdetail/dataCode/SURF_CLI_CHN_MUL_DAY_V3.0.html), and both the Global Modeling and Assimilation Office and the Goddard Earth Sciences Data and Information Services Center for the dissemination of MERRA-2 data (https://gmao.gsfc.nasa.gov/GMAO_products/reanalysis_products.php). Thanks are due to Prof. B. J. Hoskins for his constructive suggestions during communication. Thanks are also due to the anonymous reviewers whose valuable comments are important for the improvement of this manuscript. The study was supported by the National Natural Science Foundation of China Projects (41730963, 91637312, and 41905068), and the Key Research Program of Frontier Sciences (QYZDY-SSW-DQC018) and the Strategic Priority Research Program (XDB40030204 and XDB40030205) of Chinese Academy of Sciences.

There is no conflict of interest

**Appendix: Omega equation and PV advection for diabatic motion**

Under the quasi-geostrophic framework, the vorticity and temperature equations in p-coordinates can be written as:

$$(\frac{\partial}{\partial \mathrm{t}}+\vec{V}_g\cdot\nabla)\eta_g = f\frac{\partial\omega}{\partial p}, \tag{A1}$$

$$(\frac{\partial}{\partial \mathrm{t}}+\vec{V}_g\cdot\nabla)\theta = -\frac{\partial\Theta(p)}{\partial p}\omega+\dot{\theta}. \tag{A2}$$

From the hydrostatic relation:

$$\begin{cases}\dfrac{\partial\Phi}{\partial p} = -\Pi(p)\cdot\theta\end{cases} \tag{A3}$$

Eq. (A2) can be written as

$$(\frac{\partial}{\partial t}+\vec{V}_g\cdot\nabla)\frac{\partial\Phi}{\partial p}=-\Sigma^2\omega-\Pi(p)\dot{\theta}\,. \qquad \text{(A4)}$$

Eliminating vertical velocity "$\omega$" between the vorticity equation (Eq. (A1)) and temperature equation (Eq. (A4)) yields the frictionless QGPV equation:

$$(\frac{\partial}{\partial t}+\vec{V}_g\cdot\nabla)q_g=f\frac{\partial}{\partial p}(\frac{\dot{\theta}}{\Theta_p})\,. \qquad \text{(A5)}$$

Thus, for a frame of reference moving at constant horizontal velocity $\vec{C}$, the QGPV and temperature equations can be, respectively, written as

$$[\frac{\partial}{\partial t}\Big|_C+(\vec{V}_g-\vec{C})\cdot\nabla]q_g=f\frac{\partial}{\partial p}(\frac{\dot{\theta}}{\Theta_p}) \qquad \text{(A6)}$$

and

$$[\frac{\partial}{\partial t}\Big|_C+(\vec{V}_g-\vec{C})\cdot\nabla]\theta=-\Theta_p\omega+\dot{\theta}\,. \qquad \text{(A7)}$$

Applying $f\frac{\partial q_g}{\partial p}$ to Eq. (9) and using the hydrostatic relation (Eq. (A3)) and the definition of $\omega_{ID}$ (Eq. (11)) lead to:

$$L\{\omega_{ID}\}=\Sigma^2\nabla_h^2(\omega_{ID})+f^2\frac{\partial^2}{\partial p^2}(\omega_{ID})=-f\frac{\partial}{\partial p}(\frac{\partial q_g}{\partial t})\Big|_C\,.$$

From Eq. (A6), the omega equation for $\omega_{ID}$ in a diabatic atmosphere is obtained:

$$L\{\omega_{ID}\}=[\Sigma^2\nabla_h^2+f^2\frac{\partial^2}{\partial p^2}]\,\omega_{ID}=f\frac{\partial}{\partial p}[(\vec{V}_g-\vec{C})\cdot\nabla q_g]-f^2\frac{\partial^2}{\partial p^2}(\frac{\dot{\theta}}{\Theta_p})\,. \qquad \text{(A8)}$$

**References**

Aebischer, U., & Schär, C. (1998). Low-level potential vorticity and cyclogenesis to the lee of the Alps. *Journal of the Atmospheric Sciences,* 55(2), 186–207. https://doi.org/10.1175/1520-0469(1998)055<0186:LLPVAC>2.0.CO;2

Bushby, F. H. (1952). The evaluation of vertical velocity and thickness tendency from Sutcliffe's theory. *Quarterly Journal of the Royal Meteorological Society*, 78(337), 354-362. https://doi.org/10.1002/qj.49707833705

Chen, B. M., Qian, Z. A., & Zhang, L. S. (1996). Numerical simulation of the formation and development of vortices over the Qinghai-Xizang Plateau in summer (in Chinese). *Chinese Journal of Atmospheric Sciences*, 20(4), 491–502. https://doi.org/10.3878/j.issn.1006-9895.1996.04.14

Chen, S. J., & Dell'osso, L. (1984). Numerical prediction of the heavy rainfall vortex over Eastern Asia monsoon region. *Journal of the Meteorological Society of Japan*, 62(5), 730–747. https://doi.org/10.2151/jmsj1965.62.5_730

Ding, Z. Y., Liu, J. L., & Lv, J. N. (1994). The study for the mechanism of forming QXP-vortex on 600 hPa (in Chinese). *Plateau Meteorology*, 13(4), 411–418.

Djuric, D. (1969). Note on estimation of vertical motion by the omega equation. *Monthly Weather Review*, 97(12), 902-904. https://doi.org/10.1175/1520-0493(1969)097<0902:NOEOVM>2.3.CO;2

Dunn, L. B. (1991). Evaluation of vertical motion: past, present, and future. *Weather and Forecasting*, 6(1), 65-75. https://doi.org/10.1175/1520-0434(1991)006<0065:EOVMPP>2.0.CO;2

Egger, J., Hoinka, K. P., & Spengler, T. (2015). Aspects of Potential Vorticity Fluxes: Climatology and Impermeability. *Journal of the Atmospheric Sciences*, 72(8), 3257–3267. https://doi.org/10.1175/JAS-D-14-0196.1

Ertel, H. (1942). Ein neuer hydrodynamischer wirbelsatz. *Meteor. Z. Braunschweig*, 59, 33–49

Funatsu, B. M. & Waugh, D. W. (2008). Connections between potential vorticity intrusions and convection in the eastern tropical Pacific. *Journal of the Atmospheric Sciences*, 65(3),

987-1002. https://doi.org/10.1175/2007JAS2248.1

Gelaro, R., & Coauthors. (2017). The Mordern-Era Retrospective Analysis for Research and Applications, Version 2 (MERRA-2). *Journal of Climate*, 30, 5419–5454. https://doi.org/10.1175/JCLI-D-16-0758.1

Haynes, P. H., & McIntyre, M. E. (1987). On the evolution of vorticity and potential vorticity in the presence of diabatic heating and frictional or other forces. *Journal of the Atmospheric Sciences*, 44(5), 828–841. https://doi.org/10.1175/1520-0469(1987)044<0828:OTEOVA>2.0.CO;2

Haynes, P. H., & McIntyre, M. E. (1990). On the conservation and impermeability theorems for potential vorticity. *Journal of the Atmospheric Sciences*, 47(16), 2021–2031. https://doi.org/10.1175/1520-0469(1990)047<2021:OTCAIT>2.0.CO;2

Held, I. M., & Schneider, T. (1999). The surface branch of the zonally averaged mass transport in the troposphere. *Journal of the Atmospheric Sciences*, 56(11), 1688-1697. https://doi.org/10.1175/1520-0469(1999)056<1688:TSBOTZ>2.0.CO; 2

Holton, J. R. (1972). An Introduction to Dynamic Meteorology. Salt Lake City, USA: Academic.

Holton, J. R. (2004). An Introduction to Dynamic Meteorology. London, UK: Elsevier Academic.

Hoskins, B. J. (1991). Towards a PV-$\theta$ view of the general circulation. *Tellus*, 43(4), 27–35. https://doi.org/10.1034/j.1600-0870.1991.t01-3-00005.x

Hoskins, B. J., Draghici, I., & Davies, H. C. (1978). A new look at the $\omega$-equation. *Quarterly Journal of the Royal Meteorological Society*, 104(439), 31–38. https://doi.org/10.1002/qj.49710443903

Hoskins, B. J., McIntyre, M. E., & Robertson, A. W. (1985). On the use and significance of isentropic potential vorticity maps. *Quarterly Journal of the Royal Meteorological Society*,

111(470), 877–946. https://doi.org/10.1002/qj.49711147002

Hoskins, B. J., Pedder, M., & Jones, D. W. (2003). The omega equation and potential vorticity. *Quarterly Journal of the Royal Meteorological Society*, 129(595), 3277–3303. https://doi.org/10.1256/qj.02.135

Keyser, D., & Shapiro, M. A. (1986). A review of the structure and dynamics of upper-level frontal zones. *Monthly Weather Review*, 114(2), 452-499. https://doi.org/10.1175/1520-0493(1986)114<0452:AROTSA>2.0.CO; 2

Koh, T. Y., & Plumb, R. A. (2004). Isentropic zonal average formalism and the near-surface circulation. *Quarterly Journal of the Royal Meteorological Society*, 130(600), 1631–1653. https://doi.org/10.1256/qj.02.219.

Li, G. P., Zhao, B. J., & Yang, J. Q. (2002). A dynamical study of the role of surface sensible heating in the structure and intensification of the Tibetan Plateau vortices (in Chinese). *Chinese Journal of Atmospheric Sciences*, 26(4), 519–525. https://doi.org/10.3878/j.issn.1006-9895.2002.04.09

Li, G. P., Lu, H. G., Huang, C. H., Fan, Y. Y., & Zhang, B. (2016). A climatology of the surface heat source on the Tibetan Plateau in summer and its impacts on the formation of the Tibetan Plateau vortex (in Chinese). *Chinese Journal of Atmospheric Sciences*, 40(1), 131–141. https://doi.org/10.3878/j.issn.1006-9895.1504.15125.

Li, L. F., Liu, Y. M., & Bo, C. Y. (2011). Impacts of diabatic heating anomalies on an extreme snow events over South China in January 2008. *Climatic and Environmental Research* (in Chinese), 16(2), 126-136.

Liu, Y. M., Lu, M. M., Yang, H. J., Duan, A. M., & He, B. (2020). Land–atmosphere–ocean coupling associated with the Tibetan Plateau and its climate impacts. National Science Review, 7, 534–552. doi: 10.1093/nsr/nwaa011.

Ma, T., Liu, Y. M., Wu, G. X., Mao, J. Y., & Zhang, G. S. (2020). Potential Vorticity

diagnosis on the formation, development and eastward movement of a Tibetan Plateau Vortex and it's influence on the downstream precipitation (in Chinese). *Chinese Journal of Atmospheric Science,* https://doi.org/ 10.3878/j.issn.1006-9895.1904.18275.

Ma, T. T., Wu G. X, Liu Y. M., Jiang, Z. H., & Yu, J. H. (2019). Impact of surface potential vorticity density forcing over the Tibetan Plateau on the south China extreme precipitation in January 2008. Part 1: Data analysis. *Journal of Meterological Research*, 33, 400-415. https://doi.org/10.1007/s13351-019-8604-z

Nielsen-Gammon, J. W., & Gold, D. A. (2006). Dynamical diagnosis: a comparison of quasigeostrophy and Ertel potential vorticity. In L. F. Bosart, H. B. Bluestein (Eds), *Synoptic-dynamic meteorology and weather analysis forecasting: A tribute to fred sanders* (Chapter 9, pp. 183-202). Boston, MA: American Meteorological Society.

Pan, W. J., Mao, J. Y., & Wu, G. X. (2013). Characteristics and Mechanism of the 10–20-Day Oscillation of Spring Rainfall over Southern China. *Journal of Climate*, 26(14), 5072–5087. https://doi.org/10.1175/JCLI-D-12-00618.1

Petterssen, S. (1956). Weather Analysis and Forecasting. New York, USA: McGrawHill.

Reed, R. J. (1955). A study of a characteristic type of upper-level frontogenesis. *Journal of Meteorology,* 12(3), 226-237. https://doi.org/10.1175/1520-0469(1955)012<0226:ASOACT>2.0.CO;2

Rossby, C. G., & Coauthors. (1939). Relation between variations in the intensity of the zonal circulation of the atmosphere and the displacements of the semi-permanent centers of action. *Journal of Marine Research*, 2(1), 38-55.

Rossby, C. G. (1940). Planetary flow patterns in the atmosphere. *Quarterly Journal of the Royal Meteorological Society*, 66, Supplement, 68-87.

Sanders, F. & Hoskins, B. J. (1990). An easy method for estimation of Q-vectors from weather maps. *Weather and Forecasting*, 5(2), 346-353.

https://doi.org/10.1175/1520-0434(1990)005<0346:AEMFEO>2.0.CO;2

Schneider, T. (2005). Zonal momentum balance, potential vorticity dynamics, and mass fluxes on near-surface isentropes. *Journal of the Atmospheric Sciences*, 62(6), 1884–1900. https://doi.org/10.1175/JAS3341.1

Schneider, T., Held, I. M., & Garner, S. T. (2003). Boundary effects in potential vorticity dynamics. *Jouranl of the Atmospheric Sciences*, 60(8), 1024–1040. https://doi.org/10.1175/1520-0469(2003)60<1024:BEIPVD>2.0.CO;2

Shi, C. X., Jiang, J. X., & Fang, Z. Y. (2000). A study on the features of severe convection cloud clusters causing serious flooding over Changjing River Basin in 1998 (in Chinese). *Climatic Environmental Research*, 5(3), 279–286. https://doi.org/10.3878/j.issn.1006-9585.2000.03.07

Shi, N., Bueh, C., Ji, L. R., & Wang, P. X. (2008). On the medium-range process of the rainy, snowy and cold weather of South China in early 2008 Part II: Characteristics of the western Pacific subtropical high (in Chinese). *Climatic Environmental Research*, 13(4), 434–445. https://doi.org/10.3878/j.issn.1006-9585.2008.04.08

Sutcliffe, R. C. (1947). A contribution to the problem of development. *Quarterly Journal of the Royal Meteorological Society*, 73, 370-383. https://doi.org/10.1002/qj.49707331710

Tao, S. Y., & Ding, Y. H. (1981). Observational evidence of the influence of the Qinghai-Xizang (Tibet) Plateau on the occurrence of heavy rain and severe convective storms in China. *Bulletin of the American Meteorological Society*, 62(1), 23–30. https://doi.org/10.1175/1520-0477(1981)062<0023:OEOTIO>2.0.CO;2

Tao, S. Y., & Wei, J. (2008). Severe snow and freezing-rain in January 2008 in the Southern China (in Chinese). *Climatic Environmental Research*, 13(4), 337–350. https://doi.org/10.3878/j.issn.1006-9595.2008.04.01

Thorp, A. J. (1985). Diagnosis of balanced vortex structure using potential vorticity. *Journal*

*of the Atmospheric Sciences*, 42(4), 397-406. https://doi.org/10.1175/1520-0469(1985)042<0397:DOBVSU>2.0.CO;2

Thorpe, A. J., Volkert, H., & Heimann, D. (1993). Potential vorticity of flow along the Alps. *Journal of the Atmospheric Sciences*, 50(11), 1573–1590. https://doi.org/10.1175/1520-0496(1993)050<1573:PVOFAT>2.0.CO;2

Trenberth, K. E. (1978). On the interpretation of the diagnostic quasi-geostrophic omega equation. *Monthly Weather Review*, 106(1), 131-137. https://doi.org/10.1175/1520-0493(1978)106<0131:OTIOTD>2.0.CO;2

Wan, R. J., & Wu, G. X. (2007). Mechanism of the Spring Persistent Rains over southeastern China. *Science in China D: Earth Sciences*, 50(1), 130–144. https://doi.org/10.1007/s11430-007-2069-2

Wang, B., & Coauthors. (2008). Tibetan Plateau warming and precipitation changes in East China. *Geophysical Research Letters*, 35(14), L14702. https://doi.org/10.1029/2008GL034330

Wang, Z. Q., Duan, A. M., & Wu, G. X. (2014). Time-lagged impact of spring sensible heat over the Tibetan Plateau on the summer rainfall anomaly in East China: case studies using the WRF model. *Climate Dynamics*, 42, 2885–2898. https://doi.org/10.1007/s00382-013-1800-2

Waugh, D. W., & Polvani, L. M. (2000). Climatology of intrusions into the tropical upper troposphere. *Geophysical Research Lettets*, 27(23), 3857-3860. https://doi.org/10.1029/2000GL012250

Wu, G. X., & Coauthors. (1997). Sensible heat driven air-pump over the Tibetan Plateau and its impacts on the Asian summer monsoon (in Chinese). In T. C. Yeh (Eds), *Collection in Memory of Zhao Jiuzhang*, Beijing, CHN: Chinese Science Press.

Wu, G. X., Liu, Y. M., Wang, T. M., Wan, R. J., Liu, X., Li, W. P., Wang, Z. Z., Zhang, Q.,

Duan, A. M., & Liang, X. Y. (2007). The influence of mechanical and thermal forcing by the Tibetan Plateau on Asian climate. *Journal of Hydrometeorology-special section*, 8, 770-789. https://doi.org/10.1175/JHM609.1

Wu, G. X., He, B., Duan, A. M., Liu, Y. M., & Yu, W. (2017). Formation and variation of the atmospheric heat source over the Tibetan Plateau and its climate effects. *Adv. Atmos. Sci.*, 34(10), 1169–1184. doi: 10.1007/s00376-017-7014-5.

Yasunari, T., & Miwa, T. (2006). Convective cloud systems over the Tibetan Plateau and their impact on meso-scale disturbances in the Meiyu/Baiu frontal zonal. A case study in 1998. *Journal of the Meteorological Society of Japan*, 84(4), 783–803. https://doi.org/10.2151/jmsj.84.783

Yeh, T. C. (1950). The circulation of the high troposphere over China in the winter of 1945–1946. *Tellus*, 2(3), 173–183. https://doi.org/10.1111/j.2153-3490.1950.tb00329.x

Yeh, T. C., Lo, S. W., & Chu, P. C. (1957). The wind structure and heat balance in the lower troposphere over Tibetan Plateau and its surrounding. *Acta Meteorologica Sinica*, 28(2), 108–121.

Yu, J. H., Wu G. X, Liu Y. M, & Ma, T. T. (2019). Impact of Surface Potential Vorticity Density Forcing over the Tibetan Plateau on the South China Extreme Precipitation in January 2008. Part ll: Numerical Simulation. Journal of Meterological Research, 33, 416-432. https://doi.org/10.1007/s13351-019-8606-z.

Zheng, Y. J., Wu, G. X., & Liu, Y. M. (2013). Dynamical and thermal problems in vortex development and movement. Part I: A *PV-Q* view. *Acta Meteorologica Sinica*, 27(1), 1-14. https://doi.org/10.1007/s13351-013-0101-3

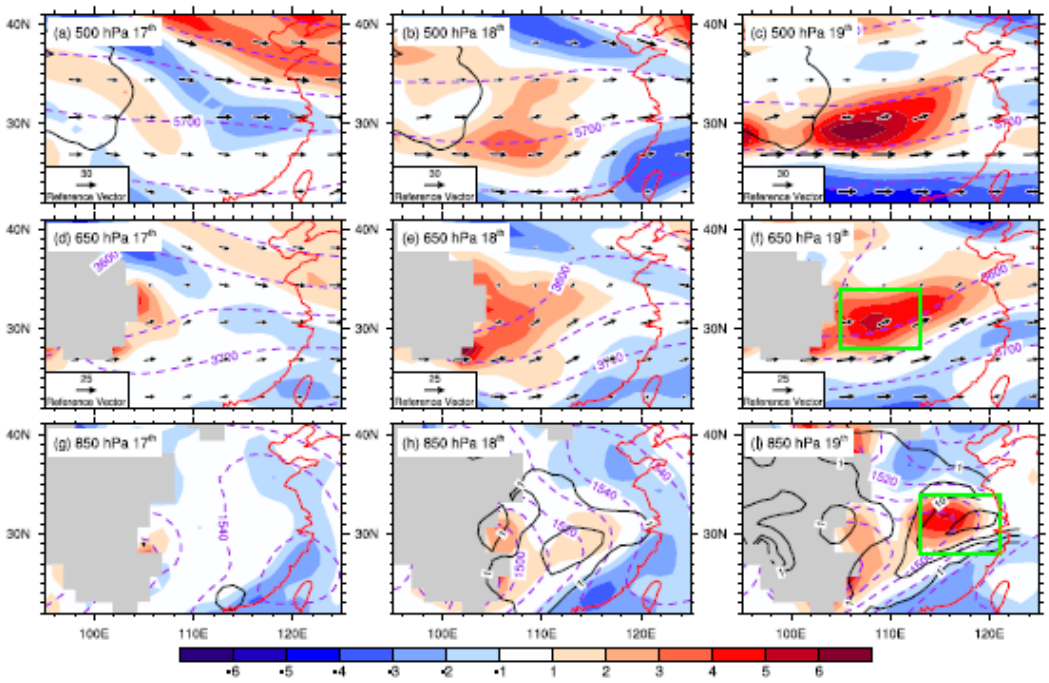


**Figure. 1.** Distributions of daily mean relative vorticity (shading, $10^{-5}$ $s^{-1}$), geopotential height (purple dashed line, m), and wind (vector, m $s^{-1}$) at (a)–(c) 500 hPa, (d)–(f) 650 hPa, and (g)–(i) 850 hPa on 17 January (left column), 18 January (middle column), and 19 January 2008 (right column). Box area V (28°–34°N, 105°–113°E) in (f) denotes the key area of relative vorticity growth, and box area R (28°–34°N, 113°–121°E) in (i) denotes the key area of precipitation and vertical velocity. Black contour in (a)–(c) indicates the elevation of 3000 m. Gray area in (d)–(i) denotes the Tibetan Plateau. Black contours in (g)–(i) indicate daily precipitation of 1, 5, 10, and 20 mm.

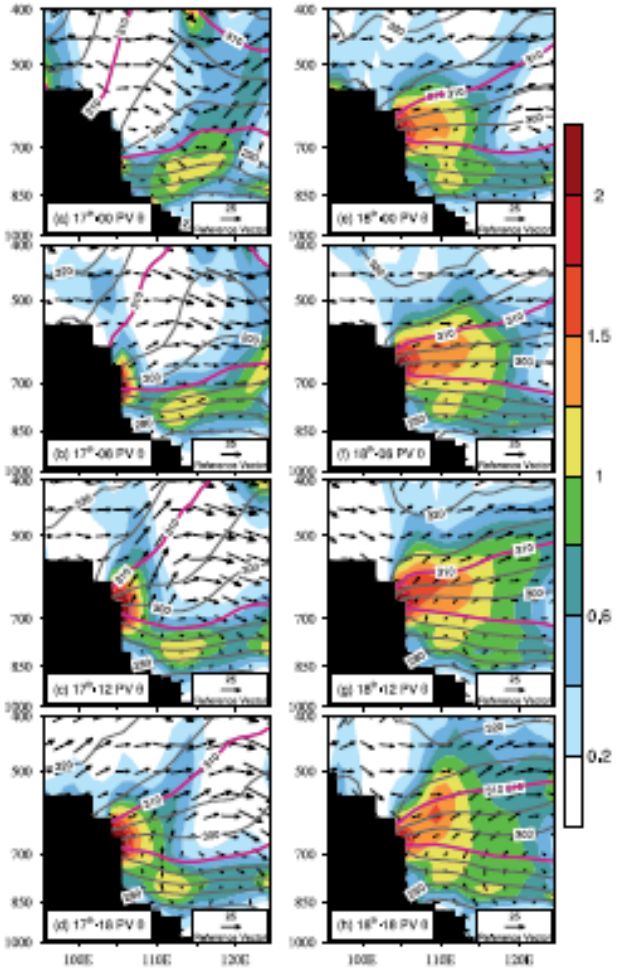


**Figure. 2.** Vertical cross section along 33°N of PV (shading, PVU; 1 PVU = $10^{-6}$ K m$^2$ s$^{-1}$ kg$^{-1}$), potential temperature (contour, K), and reanalysis wind ($u\vec{\imath} + \omega_{OB}\vec{k}$, vector, units: $u$ in m s$^{-1}$ and $\omega_{OB}$ in Pa s$^{-1}$ (values multiplied by a factor of −50)) from (a) 00 UTC on 17 January to (h) 18 UTC on 18 January 2008 at 6-h intervals. Heavy magneta contours denote isentropic temperature of 295 and 310 K.

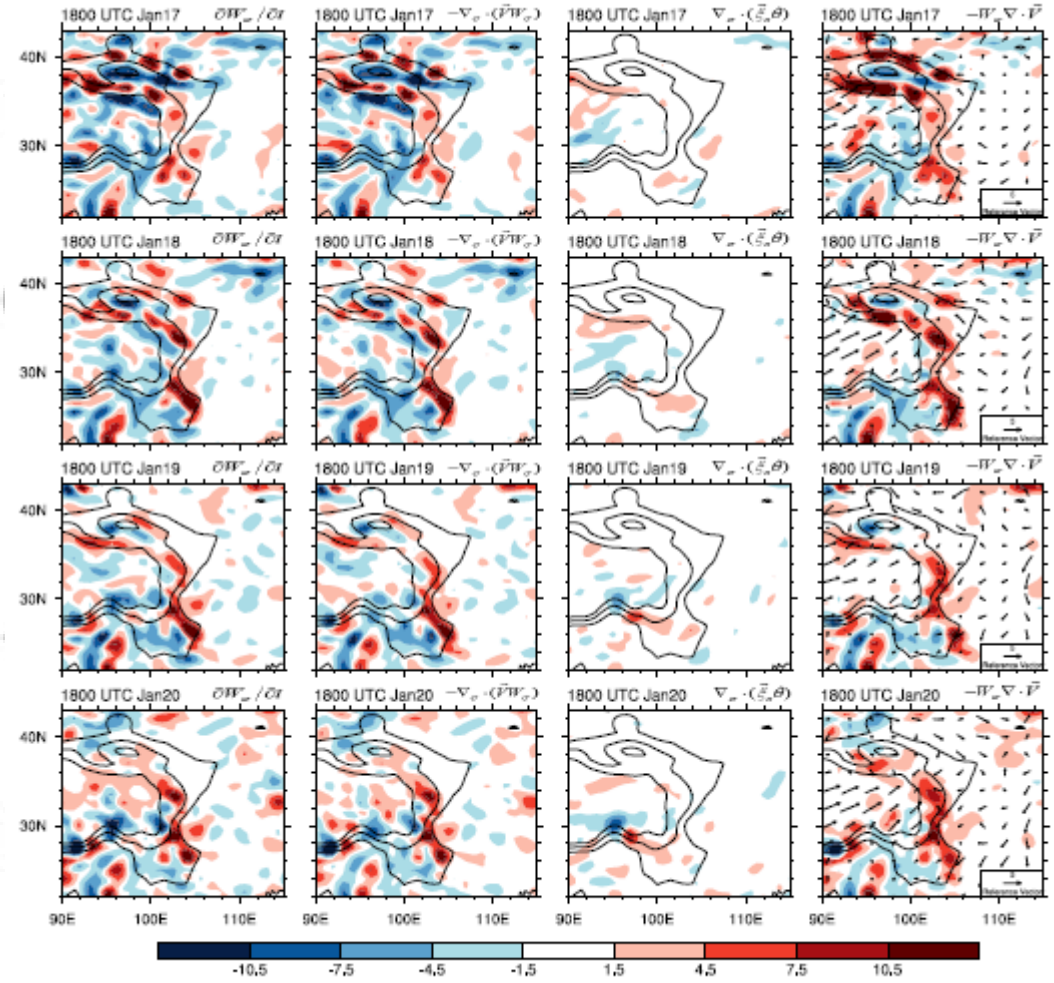


**Figure. 3.** Distributions near the surface at 18 UTC of (left column) the tendency of surface potential vorticity density ($\partial W_\sigma/\partial t$), (second column) $W$-flux divergence term ($-\nabla_\sigma \cdot (\vec{V} W_\sigma)$), (third column) diabatic heating term ($\nabla_\sigma \cdot (\vec{\xi}_{a\sigma}\dot{\theta})$), and (right column) divergence term ($-W_\sigma \nabla_\sigma \cdot \vec{V}$) and surface wind at 2 m (vector, m $s^{-1}$) from 17 January (top row) to 20 January (bottom row) 2008. Black contours indicate elevations of 1500, 3000, and 4000 m. Unit in shading is $10^{-7}$ K $s^{-2}$.

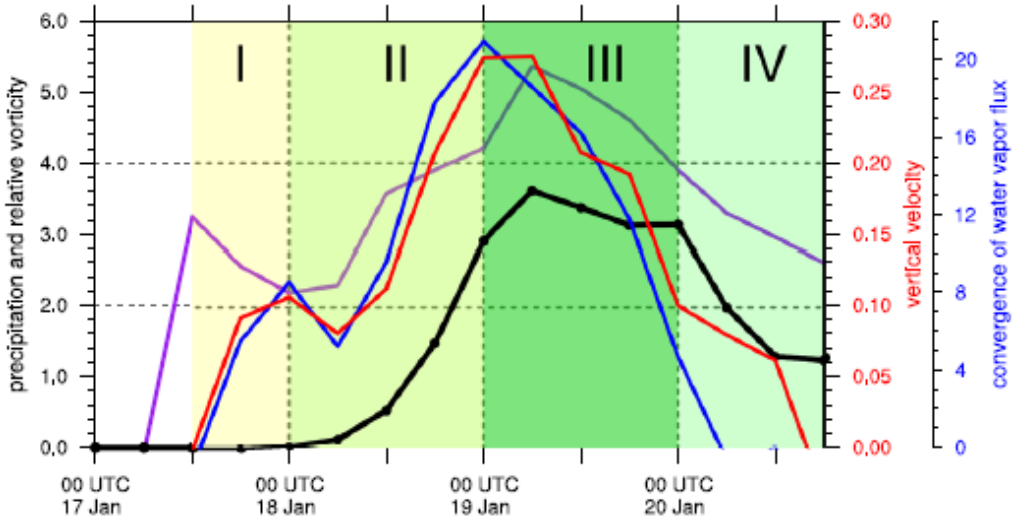


**Figure. 4.** Evolution from 00 UTC 17 January to 18 UTC 20 January of the area-mean relative vorticity (purple curve, $10^{-5}$ $s^{-1}$) at 650 hPa averaged over box area V shown in Fig. 1f; and the area-mean 6-h accumulative precipitation (black curve, mm), vertical velocity (red curve, Pa $s^{-1}$; multiplied by a factor of −1) at 650 hPa, and vertical integral of convergence of water vapor flux from the surface to 650 hPa (blue curve, $10^{-7}$ kg $m^{-2}$ $s^{-1}$; multiplied by a factor of −1) averaged over box area R shown in Fig. 1i.

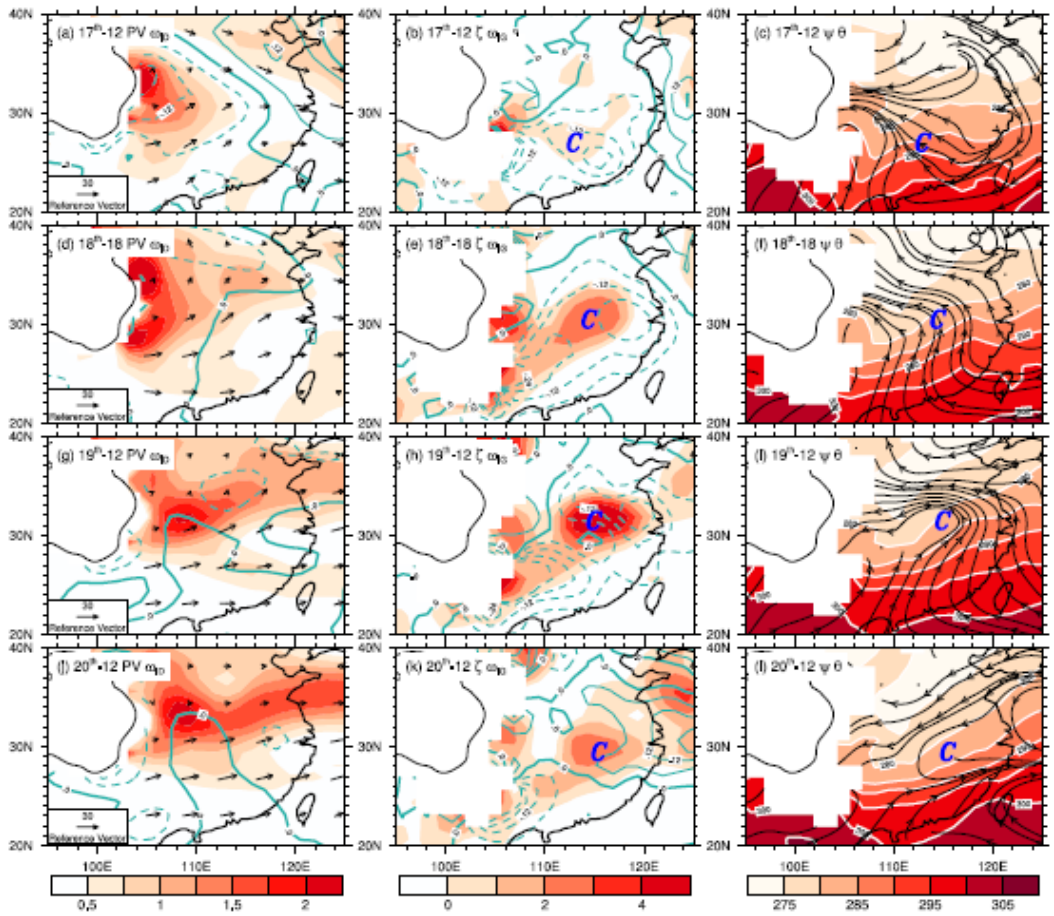


**Figure. 5.** Distributions of (left column) PV (shading, PVU) and wind (vector, m $s^{-1}$) at 650 hPa, and $\omega_{ID}$ (contour, Pa $s^{-1}$) at 700 hPa; (middle column) relative vorticity (shading, $10^{-5}$ $s^{-1}$) and $\omega_{IG}$ (contour, Pa $s^{-1}$) at 850 hPa; and (right column) potential temperature (shading, K) and circulation (streamline) at 850 hPa at (a)–(c) 12 UTC 17 January, (d)–(f) 18 UTC 18 January, (g)–(i) 12 UTC 19 January, and (j)–(l) 12 UTC 20 January. "C" denotes the cyclone circulation center at 850 hPa.

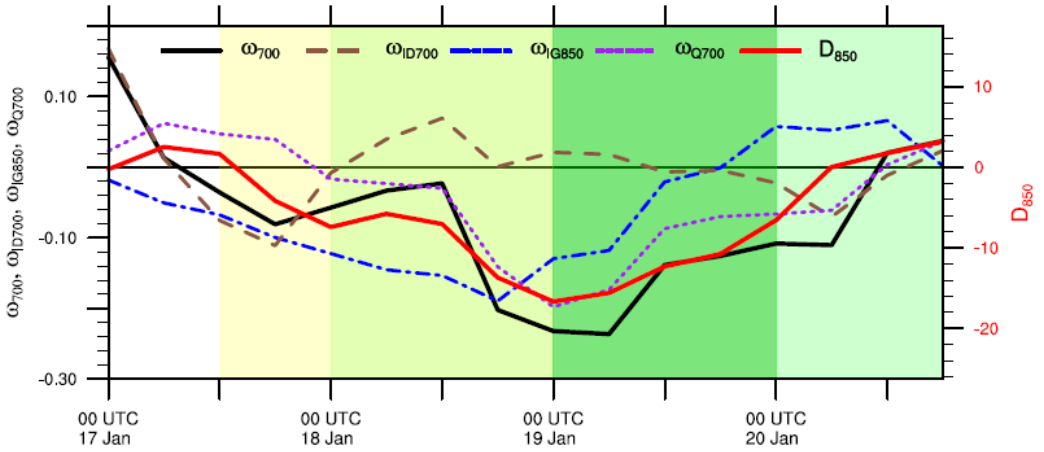


**Figure. 6.** Evolution from 00 UTC 17 January to 18 UTC 20 January at 30°N and averaged over 113°–121°E of vertical velocity ($\omega_{700}$, black curve, Pa $s^{-1}$), $\omega_{ID}$ ($\omega_{ID700}$, brown dashed curve, Pa $s^{-1}$), and $\omega_{Q}$ ($\omega_{Q700}$, purple dotted curve, Pa $s^{-1}$) at 700 hPa, and $\omega_{IG}$ ($\omega_{IG850}$, blue dashed-dotted curve, Pa $s^{-1}$) and air divergence ($\boldsymbol{D}_{850}$, red curve, $10^{-6}$ $s^{-1}$) at 850 hPa.

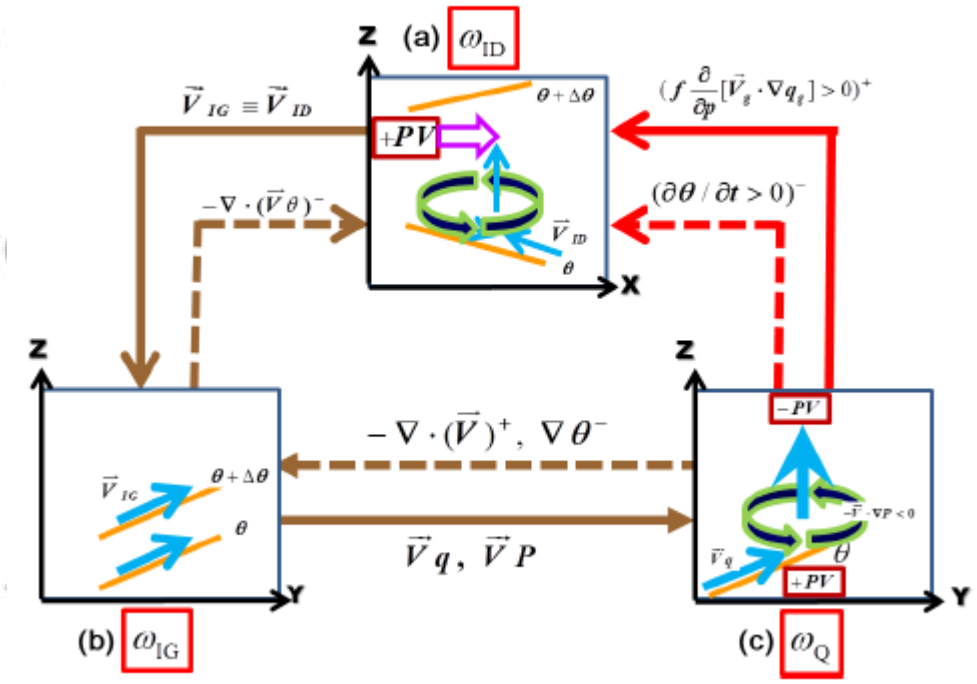


**Figure. 7.** Schematic showing the interaction among different omega components and the feedback of diabatic heating on horizontal PV advection: (a) triggering of cyclogenesis and ascending $\omega_{ID}$ by PV advection, (b) triggering of isentropic upgliding wind ($\vec{V}_{IG} \equiv \vec{V}_{ID}$) and convergence due to the development of ascending $\omega_{ID}$ and generation of $\omega_{IG}$ due to the slope of isentropic surfaces, and (c) generation of $\omega_Q$ associated with moisture transport ($\vec{V}q$) and intensification of cyclogenesis due to negative PV advection ($\vec{V}P$). Dashed brown arrows indicate positive (superscript +) and negative (superscript −) feedback mechanism; and the red solid and dashed arrows denote, respectively, positive (superscript +) and negative (superscript −) feedback of latent heating on $\omega_{ID}$. See text for more details.

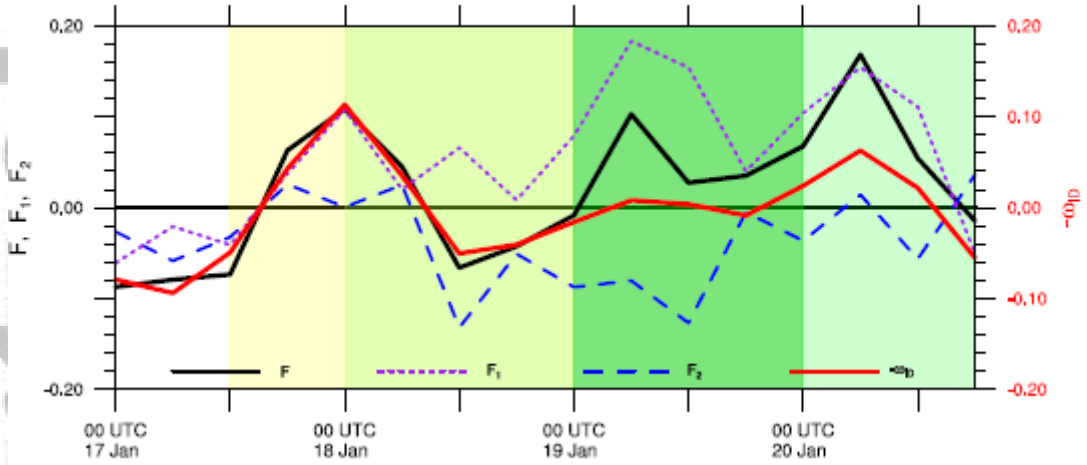


**Figure. 8.** The same as Fig. 6 but for $\omega_{ID}$ (red curve, Pa $s^{-1}$, multiplied by a factor of −1), and the sum of $\omega_{ID}$ forcing terms (F, black curve), the vertical differential advection of the quasi-geostrophic PV term ($F_1$, purple dotted curve), and the diabatic heating term ($F_2$, blue dashed curve) on the right-hand side of Eq. (14) and at 650 hPa. Unit for $\omega_{ID}$ forcing terms is $10^{-18}$ $Pa^{-1}$ $s^{-3}$.

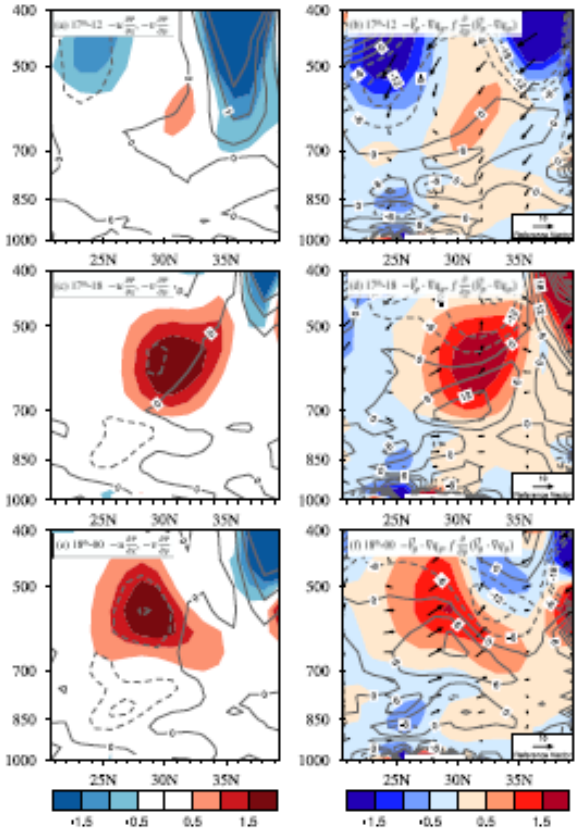


**Figure. 9.** Mean vertical cross section at 113°–121°E of (left column) zonal ($-u\frac{\partial P}{\partial x}$, shading) and meridional ($-v\frac{\partial P}{\partial y}$, contour) PV advection (interval: 0.5 × $10^{-5}$ PVU $s^{-1}$), and (right column) quasi-geostrophic QGPV advection ($-\vec{V}_g \cdot \nabla q_g$, shading, interval: 0.5 × $10^{-9}$ $s^{-2}$), $\omega$ forcing due to vertical differential quasi-geostrophic QGPV advection ($f\frac{\partial}{\partial p}(\vec{V}_g \cdot \nabla q_g)$, contour, interval: 6 × $10^{-18}$ $s^{-3}$ $Pa^{-1}$), and reanalysis wind ($v\vec{j} + \omega_{OB}\vec{k}$, vector; units: $v$ in m $s^{-1}$, $\omega_{OB}$ in Pa $s^{-1}$ (values multiplied by a factor of −50)) for (a) and (b) 12 UTC 17 January, (c) and (d) 18 UTC 17 January, and (e) and (f) 00 UTC 18 January.

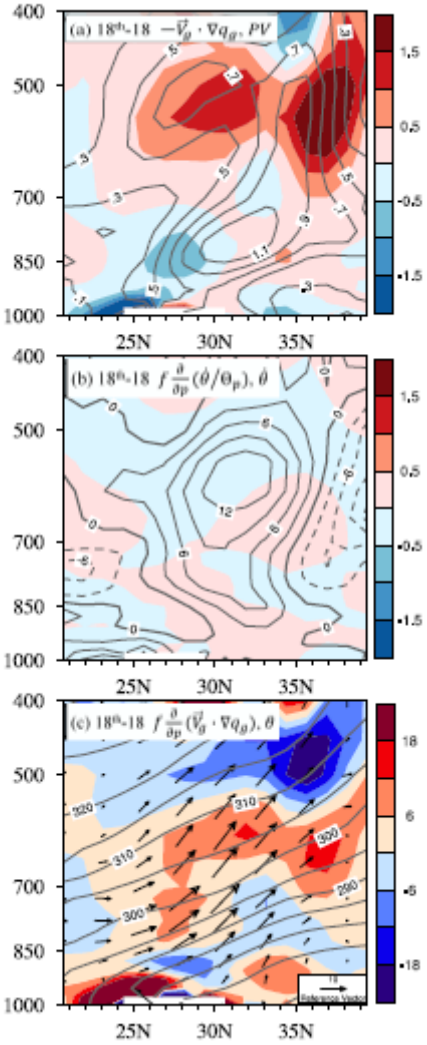


**Figure. 10.** Mean vertical cross section at 113°–121°E of (a) quasi-geostrophic QGPV advection ($-\overrightarrow{V_g} \cdot \nabla q_g$, shading, interval: 0.5 × $10^{-9}$ $s^{-2}$) and PV (contour, interval: 0.2 PVU), (b) diabatic heating term ($f\frac{\partial}{\partial p}(\frac{\dot{\theta}}{\Theta_p})$, shading, interval: 0.5 × $10^{-9}$ $s^{-2}$) and diabatic heating rate ($\dot{\theta}$, contour, interval: 3 × $10^{-5}$ K $s^{-1}$), and (c) $\omega$-forcing due to vertical differential quasi-geostrophic QGPV advection ($f\frac{\partial}{\partial p}(\vec{V}_g \cdot \nabla q_g)$, shading, interval: 6 × $10^{-18}$ $s^{-3}$ $Pa^{-1}$), potential temperature (contour, K) and reanalysis wind ($v\vec{j} + \omega_{OB}\vec{k}$, vector; units: $v$ in m $s^{-1}$, $\omega_{OB}$ in Pa $s^{-1}$ (values multiplied by a factor of −50)) for 18 UTC on 18 January 2008.

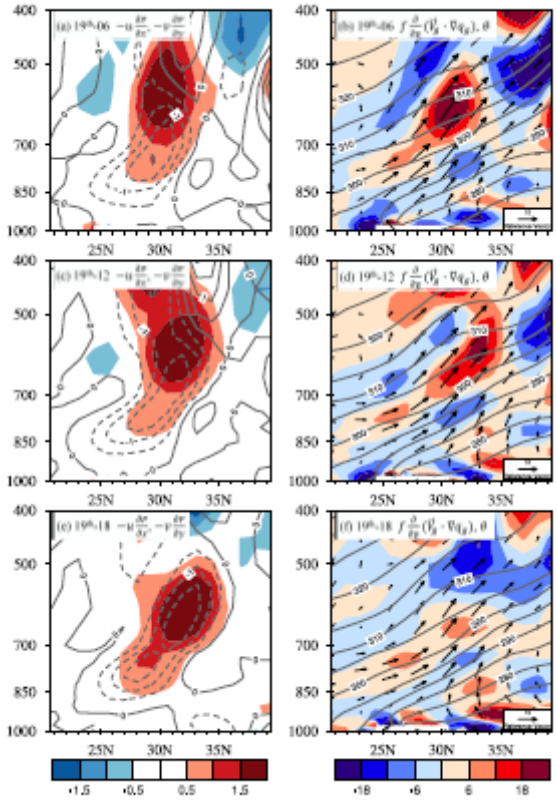


**Figure. 11.** Mean vertical cross section at 113°–121°E of (left column) zonal ($-u\frac{\partial P}{\partial x}$, shading) and meridional ($-v\frac{\partial P}{\partial y}$, contour) PV advection (interval: 0.5 × $10^{-5}$ PVU $s^{-1}$), and (right column) $\omega$ forcing due to vertical differential quasi-geostrophic QGPV advection (f$\frac{\partial}{\partial p}(\vec{V}_g \cdot \nabla q_g)$, shading, interval: 6 × $10^{-18}$ $s^{-3}$ $Pa^{-1}$), potential temperature (contour, K), and reanalysis wind ($v\vec{j} + \omega_{OB}\vec{k}$, vector; units: $v$ in m $s^{-1}$, $\omega_{OB}$ in Pa $s^{-1}$ (values multiplied by a factor of −50)) for (a) and (b) 06 UTC on 19 January, (c) and (d) 12 UTC on 19 January, and (e) and (f) 18 UTC on 19 January 2008.

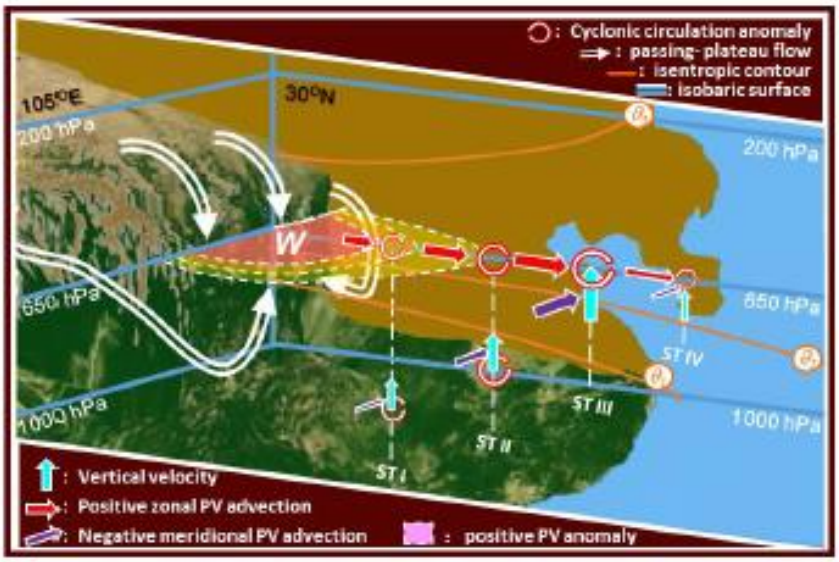


**Figure. 12.** Schematic of PV restructuring in the region of the Tibetan Plateau (TP) and the impact of PV advection on downstream circulation during different stages (ST) of cyclogenesis.

**Stage I:** Surface airflow convergence in the lee of the TP increases local PV density *W*, generating a positive relative vorticity anomaly and initiating light rain near the TP.

**Stage II:** Eastward moving positive vorticity anomaly is intensified owing to reduced static stability. Positive zonal PV advection in the mid-troposphere and increased southerly and negative meridional PV advection below enhances cyclogenesis, air ascent, and precipitation.

**Stage III:** Negative meridional PV advection is located immediately below the center of strong positive zonal PV advection, and cyclonic vorticity, vertical velocity, and precipitation are peaked.

**Stage IV:** Negative meridional PV advection tends to overlay the positive center of zonal PV advection. Consequently, the cyclone and air ascent are both weakened and precipitation is diminished.